A multi-scale analysis of the extreme rain event of Ouagadougou in 2009

Jean-Philippe Lafore, Florent Beucher, Philippe Peyrillé, Aïda Diongue-Niang, Nicolas Chapelon, Dominique Bouniol, Guy Caniaux, Florence Favot, Frédéric Ferry, Françoise Guichard, et al.

To cite this version:

Jean-Philippe Lafore, Florent Beucher, Philippe Peyrillé, Aïda Diongue-Niang, Nicolas Chapelon, et al.. A multi-scale analysis of the extreme rain event of Ouagadougou in 2009. Quarterly Journal of the Royal Meteorological Society, 2017, 143 (709), pp.3094-3109. ⟨10.1002/qj.3165⟩. ⟨hal-04917644⟩

HAL Id: hal-04917644
https://hal.science/hal-04917644v1

QUARTERLY JOURNAL
OF THE
ROYAL METEOROLOGICAL SOCIETY
RMetS
Royal Meteorological Society

A multi-scale analysis of the extreme rain event of Ouagadougou in 2009

Journal:	*QJRMS*
Manuscript ID	QJ-17-0033.R2
Wiley - Manuscript type:	Research Article
Date Submitted by the Author:	n/a
Complete List of Authors:	Lafore, Jean-Philippe; CNRM, GMME/MOANA; Beucher, Florent; Météo-France, CNRM-GMME Peyrille, Philippe; CNRM Meteo-France & CNRS, Diongue Niang, Aïda; ANACIM Chapelon, Nicolas; Météo-France, CISMF Bouniol, Dominique; Météo-France/CNRS, CNRM/GAME caniaux, guy; CNRM-GAME favot, florence; CRNM-GAME, Ferry, Frédéric; Météo-France, ENM Guichard, Francoise; CNRM-GAME (CNRS and Meteo-France), GMME/MOANA Poan, Emmanuel; Universite du Quebec a Montreal, Centre ESCER Roehrig, Romain; CNRM-GAME, Vischel, Théo; 5IGE, Univ. Grenoble Alpes
Keywords:	High-impact weather system, West Africa, African Easterly Waves, Convection
Country Keywords:	Burkina Faso, France, Senegal

A multi-scale analysis of the extreme rain event of Ouagadougou in 2009

Jean-Philippe Lafore[1], Florent Beucher[1], Philippe Peyrillé[1], Aïda Diongue-Niang[2], Nicolas Chapelon[3], Dominique Bouniol[1], Guy Caniaux[1], Florence Favot[1], Frédéric Ferry[4], Françoise Guichard[1], Emmanuel Poan[1#], Romain Roehrig[1]and Théo Vischel[5]*

[1]CNRM-UMR3589, Météo-France and CNRS, Toulouse, France
[2]ANACIM, Dakar, Senegal
[3]DP/CISMF, Météo-France, Toulouse, France
[4]ENM, Météo-France, Toulouse, France
[5]IGE, Univ. Grenoble Alpes, Grenoble, France

Abstract

This study presents a multi-scale analysis of an extreme rain event that occurred in Burkina Faso on 1st September 2009 with an absolute record of 263 mm rainfall observed at Ouagadougou. This high-impact weather system results from the combination of several favourable ingredients at different scales. The sea surface temperature anomaly patterns in July-August 2009 of both the Atlantic cold tongue, the Tropical Atlantic Dipole and the Mediterranean Sea are favourable factors for the northward penetration of the West African Monsoon. The intense convective activity of the last 10-day period in August is associated with the crossing of a convectively-coupled Kelvin Wave increasing the African easterly wave (AEW) activity, and of an Equatorial Rossby wave.

At the synoptic scale this event corresponds to the passage of a train of 3 AEWs with increasing magnitude. Behind the 1st AEW trough axis, *an intense and deep southerly monsoon burst develops. It contributes to the amplification of the 2nd AEW and its breaking associated with the formation of an intense meso-vortex on the southern flank of the African Easterly Jet. Compared to the fast moving squall-line, the dominant type of precipitating weather system over the Sahel, the Ouagadougou precipitating system appears to be a moist vortex propagating slowly, allowing*

Correspondence to: J-P. Lafore CNRM Météo-France, 42 Av. G. Coriolis 31057 Toulouse Cedex 7 France. E-mail: jean-philippe.lafore@meteo.fr

#Present address: Centre ESCER - Université du Québec, Montréal, Canada

rainfall accumulation, without wind gusts or convective cold pools observed at the surface. The main precipitation area is located about 2° longitude downshear (westward due to the African easterly jet) of the centre of this strong meso-vortex.

Keywords: High-impact weather system, West Africa, African Easterly Waves, Convection

1. Introduction

The African continent is repeatedly affected by high-impact weather (HIW) with devastating consequences for local communities. Life and property losses, damage to infrastructure (roads, bridges and buildings) and resources (energy, water supply and health sector) have been reported over the years because of HIW. In the 1970s and 1980s years severe droughts prevailed over the Sahel (Nicholson, 2001) causing famine and considerable economic losses (Benson and Clay, 1998). Within the current period of partial rainfall recovery (Lebel and Ali, 2009; Panthou *et al.* 2014), West African countries have been struck in the past decade by several floods of unprecedented magnitude (Descroix *et al.* 2012; Nka *et al.* 2015). It is the severe 2007 flood in sub-Saharan countries that brought HIW flood events to the attention of the world (Levinson and Lawrimore 2008). According to the gauge-only gridded precipitation dataset (PREC/L) of the Climate Prediction Center, a part of the National Oceanic and Atmospheric Administration (NOAA), the 2012 rainfall season was the wettest since 1952 (Thiaw 2013). The torrential rains and associated persistent flooding hit the western Sahel hardest in areas that included western Mali, the southern half of Senegal, and the Guineas. Many extreme events were reported. For instance the station of Dakar registered a record-breaking precipitation of 152 mm on 26 August (Diongue-Niang *et al.* 2017). Also in 2012, the Middle Niger River exhibited the highest flood level ever registered from the beginning of its monitoring in 1929 (Sighomnou et al. 2013).

A key question is to understand what determines the predictability of these events, for which both individual cases and statistical studies are needed. In the framework of THORPEX[1] (THe Observing Research and Predictability Experiment), the THORPEX-Africa regional committee has selected a few cases related to flooding events to study their predictability. To achieve this task, three steps have been defined: i) description and conceptual model of case studies, ii) verification of

---

[1] www.wmo.int/thorpex

forecasts and the assessment of model ability to predict such events, iii) modelling studies to further analyse the predictability of such events. This paper aims at tackling the first item for the case study selected for the West African sub-region. It is part of a wet spell in the Sahel with an extreme rainfall event that occurred in Ouagadougou (Burkina Faso) on 1st September 2009, with 263 mm recorded in ten hours. This led to 150 000 people being displaced (of 1.5 million inhabitants), 9 deaths, extensive loss of property and damaged roads.

Several observational and numerical studies have been performed to document and better understand rainfall events in West Africa. They are based on case studies from field campaigns such as COPT81 (Chong *et al.* 1987; Roux 1988; Redelsperger and Lafore 1988), HAPEX-Sahel (Redelsperger *et al.* 2002; Diongue *et al.* 2002), or more recently the AMMA SOP2006. Case studies such as presented in Barthe *et al.* (2010), Chong (2010) Schwendike and Jones (2010) Birch *et al.* (2012), Beucher *et al.* (2013) focused more particularly on the interactions between mesoscale systems and synoptic disturbances such as African Easterly Waves (AEWs) which are key synoptic weather systems affecting West Africa during the monsoon (Fink and Reiner 2003). These studies mainly addressed fast-moving squall lines that are the dominant type of rain event over the semi-arid Sahel region (Mathon *et al.* 2002). They contribute up to 80 % of the annual regional rainfall over the Sahel (Le Barbé *et al.* 2002; D'Amato and Lebel 1998). They often generate intense precipitation and strong wind bursts associated with intense cold pools fed by rain evaporation. Nevertheless due to their fast propagation, the passage of a squall-line over a given location is short, typically from about 1/2h to 2h for the convective and stratiform parts, respectively (see the recent mesoscale convective systems (MCS) statistics over West Africa of Lafore e*t al.* 2017, Fig. 3.16). This short duration may explain why the observed accumulated rainfall rarely exceeds the precipitable water (PW) ahead of the squall-line (typically 50-65 mm over the Sahel during the monsoon season, Poan et al. 2013). For instance the maximum accumulated precipitation recorded were 47 and 37 mm for the passage of a squall-line during COPT81 and Hapex-Sahel field experiments, respectively (Chalon *et al.* 1988; Redelsperger *et al.* 2002), whereas the PW ahead of the squall-line was about 55 mm for both cases. Le Barbé *et al.* (2002) found a mean accumulated rainfall per MCS of ~15 mm at Niamey. To reach a daily accumulated rainfall above PW, the system must be very efficient in concentrating water vapour for a long duration at a given location due either to a slow propagation, a forcing mechanism by the topography or the large-scale dynamics. As observed extreme rainfall events reach values above 100 mm per day at a given location (Panthou *et al.* 2012), it raises the following questions: Are the physical processes involved in Sahelian extreme rain events different from the ones involved in squall-lines? What are their temporal and spatial scales?

There is, however, a lack of studies of such HIW rain events to help answer these questions. Among the few related studies, Paeth et al. (2011) performed an analysis of the 2007 flood caused by a sequence of strong rain events in August and September. They first assessed the structure and intensity of the flood and of associated rain event sequences from various observational data sets. Estimated return times from the Tropical Rainfall Measuring Mission range between 1 and 50 years for daily precipitation, but have a high spatial heterogeneity and a maximum over the Upper Volta Basin. Burkina Faso appears as a hot spot for flood-producing rain events from August to September.

Another question is: what are the contextual elements of the climate conditions in which HIW rain events may occur? To help answer this question, Nicholson (2009) proposed a conceptual framework for studying rainfall variability over West Africa resulting from two distinct modes: *latitudinal displacements* of the tropical rain belt and changes in its *intensity*. From this arise four patterns of rainfall anomalies: "non-dipole" years when anomalies are of the same sign over most of West Africa due to a change in rain belt intensity, whereas anomalies are of opposite sign in the Sahel and the Guinea Coast during "dipole" years due to latitudinal displacements (see Fig. 1 of Nicholson 2009). In this framework, 2007 is a “wet non-dipole" year (Paeth et al. 2011), whereas 2009, 2012 and 2013 are “wet dipole” years (see State of Climate in corresponding years; Thiaw 2013).

The above framework proposes some large-scale factors favouring wet or dry years for the WAM, but we do not know if the probability of occurrence of HIW rain events is stronger during wet years than in dry years. Also, these HIWs are not excluded from a dry year. So far there is no clear understanding of the atmospheric conditions leading to a HIW rain event.

At the regional scale, Crétat *et al.* (2015) analysed the relationship between AEW and daily rainfall over West Africa and concluded that 3-5-day AEWs establish the most favourable synoptic conditions for the development of intense rainfall events. This is consistent with previous work showing that the AEW activity is enhanced during wet years (Grist 2002; Grist *et al.* 2002; Nicholson 2009; Paeth *et al.* 2011). Ventrice and Thorncroft (2013) showed that the AEW activity increases at the leading edge and during the convectively active phase of strong Convective Coupled Kelvin Waves (CCKWs). Ventrice *et al.* (2011) also suggested that the Madden-Jullian oscillation (MJO) directly influences AEW activity. During MJO phases 8, 1, and 2, diagnosed by the Wheeler and Hendon (2004) Realtime MJO Multivariate (RMM) index, the AEJ increases and convection is enhanced over tropical Africa, whereas AEW activity is locally enhanced during phases 1-3. According to these studies, equatorial waves (CCKW and MJO at least) can modulate the environment on which AEWs develop, *i.e.* the magnitude of the AEJ, the vertical wind shear, the low-level convergence and vorticity patterns. Since the AEWs are the leading driver of the most intense storms, a connection is possible between equatorial waves and HIW. The present paper actually shows that this link exists which opens interesting forecasting perspectives (See section 4).

If a better understanding of extreme rainfall events is a crucial issue in better forecasting them, another issue is the trend in their occurrence and intensity in the context of ongoing global warming (Westra *et al.* 2014). At a regional scale, in the Sahel, Panthou *et al.* (2014) found that the partial recovery of rainfall is more likely due to the increase in the number of intense events (increase of 33% between 2001-2010 and 1970-1990), than the increase in the total number of events (3% of increase in the same periods). Taylor et al. (2017) also found that the frequency of extreme Sahelian storms tripled since 1982 in satellite observations.

The main goal of this first paper is to present a multi-scale analysis of the extreme rain event of Ouagadougou that occurred on 1st September 2009, with a focus on regional and synoptic scales and to identify key factors for this type of event. This case has been used in the recently published West African Forecaster's Handbook (Parker and Diop-Kane, 2017) to illustrate AEW breaking events (Cornforth *et al.* 2017) as seen by forecasters. In a companion paper we will analyse the physical mechanisms involved in the small-scale development of a moist vortex associated with this extreme rain event, owing to the computation of budgets of heat, moisture and vorticity from a convection-permitting simulation.

After a description in section 2 of the datasets used in this study, section 3 describes the characteristics of this extreme event and the large-scale context it is embedded in. Section 4 focuses on wave activity, more specifically on AEWs and on the impact of equatorial waves on this event.

The convective organization is analysed in section 5. Section 6 summarizes the main findings and proposes a list of factors favouring the occurrence of this type of event associated with the breaking of an AEW.

2. Data and analysis methods

a. *Observations*

In the frame work of THORPEX-Africa, daily rain-gauge data of a network of 579 stations have been kindly provided by National Weather Services of most West African countries impacted by this wet spell. This rain-gauge network data covers a 20-day period centred on 1st September 2009 to document this period of intense precipitation (see subsection 3.a) in which the Ouagadougou event is embedded.

This dataset is very valuable for the present study and for further ones to assess the numerical weather prediction (NWP) system's skill to forecast such extreme events. In addition, the Tropical Rainfall Measuring Mission (TRMM-3B42) rainfall estimates (Huffman *et al.*, 2007) have been used. To complement this, the Global Satellite Mapping of Precipitation (GSMaP) v5 satellite estimate of 0.1° x 0.1° gridded 1h accumulated precipitation (Ushio *et al.*, 2009) is used to track MCSs.

The convective activity and its spatial structure have been analysed by computing the Polarized Corrected Temperature (PCT) parameter (Mohr and Zipser 1996) from snapshots provided by AMSR-E (Advanced Microwave Scanning Radiometer - Earth Observing System), SSMI (Special Sensor Microwave Imager) and TMI (Special Sensor Microwave Imager) microwave radiometers. PCT also allows the identification of convective and stratiform regions. Daily-averaged outgoing longwave radiation (OLR) data provided by the NOAA polar-orbiting satellites (Liebmann and Smith 1996) was used as a proxy for convective activity.

To assess the oceanic state in 2009, sea surface temperature (SST) anomalies during July-August 2009 have been computed from the Reynolds climatology over the 33-year period (1982-2014) (Reynolds *et al*. 2002). The soundings of Abidjan [5.18°N,4°W] performed twice a day have been used to assess the presence of equatorial waves.

b. *Reanalysis*

The present study is partly based on the last (‘Interim’) European Centre for Medium-Range Weather Forecasts (ECMWF) Reanalysis (Dee *et al.*, 2011, ERA-I hereafter). To improve the analysis in a region of sparse observations such as Africa, we assimilated remote-sensing microwave data from AMSU-B, by using the method developed by Karbou *et al.* (2010a) as in Beucher *et al.* (2013). We performed a 4D-Var assimilation with the global ARPEGE operational model of Météo-France (Courtier *et al.*, 1994). The 4D-Var assimilation experiment was performed over a ~1 month-period (13 August to 10 September 2009), four times per day, with the April 2010 version (T798 truncation and a stretched horizontal grid allowing a ~15 km resolution over Africa). Thanks to its finer horizontal resolution and AMSU-B data, we used the ARPEGE reanalysis in this paper for a more accurate analysis of the synoptic scale in section 4 (see Karbou *et al.* 2010b, Beucher *et al.* 2011 for a comparison between ERAI and ARPEGE), in addition to ERA-I.

c. *Analysis methods*

As done for instance by Takayabu (1994) or Wheeler and Kiladis (1999), a zonal space-time spectral analysis is performed to detect and analyse equatorial waves concomitant with the present extreme precipitation event. Following Roundy and Franck (2002) and Schreck *et al.* (2012), the spectral analysis is made for each latitude between 30°S and 30°N and filtered in the wavenumber – frequency domain without imposing equatorial symmetry to the data. Table 1 summarizes the characteristics of the filters used to extract the Madden-Julian oscillation (MJO), Kelvin (K), Equatorial Rossby (ER), and westward Mixed Rossby-Gravity (MRG) waves. We added the Tropical-Depression-type (TD-type) disturbances that correspond to AEWs over Africa. The filtering is applied to either the 200-hPa velocity potential seasonal anomalies, OLR seasonal anomalies or the mass-weighted 950-600 hPa layer-averaged meridional wind (hereafter meridional mass transport) depending on the wave-type (Table 1). The equivalent depths used for the wave filtering are 8-90 m for ER, Kelvin and MRG (Wheeler and Kiladis, 1999) and no equivalent depth is imposed for the MJO and TD-AEW.

We developed an AEW tracking based on the barotropic flow (mass weighted mean wind between 950-600 hPa) as a two-step procedure: (i) the detection of the maximum relative vorticity provides a "first guess" for the tracked pattern, (ii) a finer spatial localisation by searching for the minimum wind speed corresponding to the centre of the barotropic flow. This method is applied at an hourly frequency to ARPEGE re-analysis and simulations, at 15 km horizontal resolution (See Section 5).

3. Main characteristics of the extreme event and large-scale context

a. *Precipitation*

The case study occurred during a wet spell that affected the whole Sahel during the 20-day period from 21st August to 10th September 2009, marked with heavy precipitation leading to floods in many Sahelian countries (notably in Niger, Senegal, Mauritania, Gambia – see State of Climate in 2009, by Arndt et al., 2010). The event that occurred in Burkina Faso on September 1st, caused by a slow-moving MCS (see section 5), has been the most extreme ever observed over the Western Sahel. Between 0400-1600 UTC 263 mm were recorded at Ouagadougou, the capital city. The accumulated hourly rainfall peak (97 mm) occurred between 0700-0800 UTC. The 30 rain records collected over Burkina Faso on 31 August and 1st September (Fig. 1a) provide an idea of the size, intensity and trajectory of this extreme event. The pattern of the corresponding accumulated rain as estimated by TRMM (red isolines) is in agreement with rain gauge records, although underestimated (by a factor 2 for the maximum) probably partly due to the difference in scale. The Ouagadougou extreme event affected an area of about 150x100 km^2 with accumulated rain above 75 mm (50 mm for TRMM). For the 15 stations at a distance less than 1° from Ouagadougou, the mean accumulated rainfall was 94 mm (117 mm for the 7 stations at a distance less than 0.5°) and the second highest record reached 213 mm at Boulbi (13 km south of Ouagadougou). TRMM estimates reached a maximum of 110 mm close to Ouagadougou. TRMM suggests that this event also generated important precipitation (above 75 mm) during the previous night over eastern Burkina, but the density of the rain gauge network was too sparse to confirm this finding. Figure 1b shows observed extrema of daily precipitation over West Africa during the 20-day period from 21st August to 10th September, with the indication of values above 100 mm/day (red points) and their date of occurrence. The Ouagadougou case is the absolute observed maximum (263 mm with a return period estimated at 10 000 yrs by Karambiri 2009) of the 22 recorded strong events. Here, we consider that en event is strong when the daily precipitation reaches more than 100 mm, *i.e.* when it produces much more precipitation than the amount of water vapour stored in the column (PW_{max} ~65 mm, Poan *et al.* 2013, Lafore *et al.* 2017). This is likely a large number as Panthou *et al.* (2012) estimate that the return time for a 100 mm daily precipitation is 15 and 20 years at Ouagadougou and Niamey, respectively. Those strong events in 2009 are clustered over specific regions (Senegal, South of Mauritania in particular) and periods corresponding to the passage of AEWs as shown later in section 4a. The TRMM accumulated rain over this 20-day period (Fig. 1c) agrees well with rain-gauge observations (Fig. 1d) at this scale. It is to be noticed that regions with intense daily events (Fig. 1b) correspond to regions of maximum accumulated rain over the 20-day period, suggesting a major contribution of intense events to the seasonal rainfall (which is consistent with Panthou *et al.* 2012). Fig. 1e shows the TRMM accumulated rainfall at the monsoon seasonal scale (July-August-September, JAS hereafter) and Fig. 1f its anomaly relative to the 1998-2012 TRMM climatology. Clearly 2009 appears as a wet dipole year over the Sahel (up to ~+300 mm). At the seasonal scale the rainfall anomalies are located over Senegal, South of Mauritania, Mali and Niger, where intense events (above 100 mm/day) occurred during the active 20-day period of August and September (Fig. 1d), suggesting a significant contribution of intense events to the seasonal rainfall anomaly.

b. SST pattern

At very large-scale, 2009 was characterized by the transition between a waning Pacific La Niña and the establishment of a strong El Niño event from June 2009 to April 2010 (Arndt *et al.*, 2010). In 2009, the Atlantic Ocean was warmer in the northern hemisphere due to the warm phase of the Atlantic Multi-decadal Oscillation (AMO, Enfield and Mestas-Nunez 1999) which has resulted in greater Atlantic hurricane activity since 1995.

Figure 2 displays SST anomalies surrounding Africa for July-August 2009. A dipole is present in the North Atlantic with warm anomalies (2°C) in the north-western Atlantic and anomalies colder than -2°C eastward. The cold anomalies in the north-eastern Atlantic are the signature of a negative North Atlantic Oscillation (NAO) index for the July-August period. In the tropical Atlantic, a positive Atlantic dipole (Lamb 1978, Parker *et al.*, 1988; Servain, 1991) is present with a cold anomaly (down to -1°C) along the equator, which also affects the Atlantic cold tongue in the eastern equatorial basin. Based on the climatological indices defined by Caniaux *et al.* (2011), the cold tongue was colder and more extended in July-August 2009 than the climatology (not shown).

Combined with the AMO warm phase, a colder Atlantic cold tongue and a resulting positive Tropical Atlantic SST dipole are favourable conditions for the northward penetration of the WAM into the West African continent. The warm anomaly in the Mediterranean Sea (Fig. 2) can also be considered as a favourable factor (Rowell, 2003; Peyrillé *et al.* 2007).

The warm SST anomaly in the Indian Ocean (Fig. 2) started at the same time as the Pacific El Niño in 2009, instead of one year later as more commonly found (*e.g.*, in 1998, 1987 and 1983; Arndt *et al.* 2011). A statistical relationship has been found linking a warm anomaly in the Indian Ocean to dry conditions over the Sahel in the last decades (Giannini *et al.* 2003; Bader and Latif 2003), such that the warm anomaly over the Indian Ocean should not have favoured moister conditions over the Sahel in 2009. Recent studies indicate, however, that this link might not be straightforward for the last decade with the recent phasing of the NAO and ENSO (Joly *et al.* 2007; Rodriguez-Fonseca *et al.* 2011).

To summarize, the SST anomaly patterns in July-August 2009 of the Atlantic cold tongue, the Tropical Atlantic Dipole and the Mediterranean Sea are favourable factors for the WAM northward penetration. They are consistent with the classification of 2009 as a “Dipole wet year” (Nicholson 2009). However, the impacts of El Niño, Indian Ocean warming and negative NAO on the WAM deserve more analysis.

c. Multi-scale nature of the event

Figure 3a analyses the seasonal evolution of the TRMM mean rainfall in 2009 in the 1° square around Ouagadougou [12 – 13°N; 2 – 1°W] (red square in Fig. 1). The passage of the extreme Ouagadougou event is clearly seen at the daily and box scales (up to 72 mm/day). This extrem rain event significantly contributes to the positive anomaly of accumulated rain observed in 2009 at Ouagadougou. Another active period is observed from late June to early July. When compared to the TRMM (1998-2012) climatology, 2009 rainfall is weaker in June and July, which corresponds to a late onset, but the deficit is made up and reversed during the very active period of August-September. The wavelet analysis (Fig. 3b) reveals that 4 bands are active at synoptic (3-5 days), short (10-15 days), medium (20-30 days) and long (40-80 days) intraseasonal scales. The Ouagadougou extreme event thus occurs at a time when all these scales of variability are strong (this is also true of the active period of late June-early July). It suggests that this extreme event corresponds to the superposition of favourable conditions at different temporal scales.

4. Propagating modes of variability and wave activity

a. AEWs

Figure 4 provides a synoptic view of the Ougadougou event over a 3-day period at two key levels to identify AEWs: at low levels (925 hPa, right) and at the AEJ level (700 hPa, left). At 700 hPa the AEJ is well defined in the 10 – 20°N band with a maximum intensity above 20 ms^{-1} (Fig. 4a, b, c). Its oscillations correspond to a train of 3 AEWs, and increase during this 3-day period. On 30th August, the first AEW of this series is well formed with its trough T1 located over Burkina Faso (red line in Fig. 4a). A fast-moving squall-line propagates ahead of T1 in the AEJ core (pink shading). The trough T1 propagates westward and reaches the coast two days later. An important feature at 700 hPa is the development of a strong southerly flow behind T1 coming from the southern hemisphere. The signature at low levels is a westerly flow west of T1 and an intense south-westerly monsoon flow east of T1 (Fig. 4d, e, f). The combination of these strong southerlies behind

T1 at low levels and at the AEJ level is a deep southerly burst maximum on 31st August. This is associated with the development of a deep and strong ridge R1 (dotted red line in Fig. 4) behind T1. Quite unusually, this southerly burst is so strong that it brings dry air from the southern hemisphere and generates a dry anomaly (dark shading in Fig. 4d, e, f) in the R1 region.

A second wave develops behind this first AEW (T1 and R1). Its trough T2 appears just west of Lake Chad on 30th August (Fig. 4a), on the south-western flank of a widespread wet anomaly (light-gray shading in Fig. 4d). One day later (Fig. 4b, e) T2 appears as a small-scale cyclonic circulation both at 700 and 925 hPa, such that we have an almost barotropic vortex structure which reaches its maximum on 1st September (Fig. 4c, f). On this date, this vortex located over Niamey has wrapped the wet anomaly which almost splits it into two parts (grey area in Fig. 4f). A key feature of this event is that contrary to the usual schematic of an AEW (Cornforth *et al.* 2017 – see their Fig. 2.10) the wet anomaly is ahead (west) of the trough T2 within the northerly flow, instead of being located behind the trough in the monsoon flow. The effect is that the vortex is moistened by the northerly flow. The extreme rain event (coloured shading in Fig. 4c, f) occurred over the Ouagadougou region, 2° west of the vortex within the wet anomaly.

To complete, Figure 5 shows a longitude-time diagram zoomed between 40°W and 40°E from 20th August to 10th September for (a) the relative vorticity at 700 hPa and (b) the anomaly of PW. Fields are averaged in the Sahelian band [10 – 18°N]. The passage of the train of 3 AEWs is clearly identified in the vorticity field (Fig. 5a). The first trough T1 corresponds to the wet spell arrival (Fig. 5b) and is followed by the strong ridge R1 (anticyclonic vorticity) along the Greenwich meridian. The second trough T2 is even stronger. A day later on 31st August, T2 accelerates and reaches Ouagadougou on 1st September. A third trough T3 intensifies on 4th September near the Greenwich meridian and coincides with the maximum of the wet spell (PW > 60 mm in Fig. 5b). It is also the most intense trough within the wave train in terms of vorticity signature. This sequence of three successive waves of increasing intensity is consistent with the AEW amplification mechanism due to their upstream group velocity (Diaz and Aiyyer 2013). T3 later reaches the Atlantic Ocean and gives rise to Hurricane Fred on 7th September at 1800 UTC reaching its maximum intensity (958 hPa, 53 m s^{-1}) 2 days later (see NHC report[2]). The trajectory of Fred follows the maximum of PW anomalies and vorticity associated with the trough T3 (doted line T3 in Fig. 5). The cyclonic vorticity intensification is in general preceded by a reinforcement of the AEJ (Fig. 5a), which is consistent with Leroux *et al.* (2009), suggesting that an intense AEJ is necessary for intense AEWs to develop. It is to be noticed that the vorticity maximum in the eastern Sahel occurring on 26-27th August corresponds to an AEJ reaching 17.5 ms^{-1}, much stronger than its climatological value from the ERA-I reanalysis (9 ms^{-1}, not shown).

To track the deep southerly burst noted in Fig. 4, we computed the meridional mass transport Figure 5c). It provides a clear signature of well organized AEWs, with the trough located between the deep northerly wind and the southerly deep monsoon flow (to the west and the east, respectively).

b. Equatorial wave activity

Anomalies of velocity potential at 200 hPa (VP_{200} - Fig. 6a) and of OLR (Fig. 6b) from 1st August to 10th September 2009 emphasize favourable large-scale conditions for convection prevailing over West Africa, in agreement with Fig. 3a. The analysis of the contributions of equatorial waves (MJO, Kelvin and Rossby) to the anomalies of VP_{200} and of OLR (isolines overlaid in Fig. 6) provides additional information. The different signatures obtained using either the VP_{200} or OLR show that the waves are identified slightly differently depending on their life cycle and on the degree of coupling between convection and the dynamics. However the two panels (Fig. 6a and b) show consistent propagation of the envelop of equatorial waves.

---

[2] http://www.nhc.noaa.gov/data/tcr/AL072009_Fred.pdf

During the first 10 days of August, a large divergence anomaly is centred over eastern Pacific and America, possibly favoured by the intensifying El Niño, whereas a weakly eastward-propagating suppressed convection phase (convergence anomaly) is located over the Indian Ocean. The favourable phase for convection mainly propagates eastward as a convectively-coupled Kelvin wave (K1), detected both in VP_{200} and OLR anomaly fields. K1 reaches Africa between 10th and 20th August and is associated with intense convective activity. An MJO signal is also detected over Africa in the middle of August. An equatorial Rossby wave (ER) coming from the Indian Ocean reaches East Africa and then crosses Africa during the last 10 days of August. Meanwhile K1 travels from Maritime continent, to the Atlantic Ocean, where a second Kelvin wave (K2) is generated. The Ouagadougou extreme precipitation event (black circles) coincides with the crossing of the equatorial Rossby wave ER and the Kelvin wave K2. Overall, the MJO signal, which continues eastward over the Maritime Continent, remains weak during the period (after RMM index, not shown). The similar patterns of the waves (Kelvin and ER) detected from the OLR and velocity potential anomalies (Figs. 6b and 6a) shows that the detection of convectively-coupled waves is consistent.

In the present case the AEW wave train corresponds to the passage of the wet spell, and its amplification appears to start after the crossing of the Kelvin wave K2 and the Rossby wave ER (Fig. 6, Fig. 5c). The following sub-section 4.c analyses the influence of equatorial waves on this extreme event.

c. Connection between equatorial waves and AEWs

Figure 7 shows maps of meridional mass transport (shading) along with the contribution of ER, MRG and AEW waves to this field (isolines) during the 3-day period from 30th August to 1st September. The evolution of the meridional mass transport shows the propagation of strong northerlies – between R1 and T2 – from 10°E on 30th August to the longitude of Ouagadougou on 1st September, on which the Ouagadougou convective system develops, bordered by strong southerlies to the west and weaker southerlies to the east. As mentioned in Fig. 4, the propagation of this dipole of northerly and southerly winds over the Sahel is key to the event and is largely explained by the propagation of an AEW train (Fig.7a, b, c). The AEWs even explain a large part of the signal very far into the southern hemisphere, down to 10°S, consistently with Kiladis *et al.* (2006, *e.g.*, their Fig. 3). The ER wave which develops further to the east at 15°E (Fig. 7d, e, f) also contributes to the southerly anomaly, but does not seem to reinforce the AEW at the longitude of the event. This will be further discussed with Fig. 8. The MRG wave contributes to the southerlies between T1 and R1 on 30 and 31 August (Fig. 7g, h). It is in phase with the AEW during these two days and thus reinforces the AEW. The maximum contribution of the MRG wave is in the 5–10°N band (Fig. 7g, h, i), which suggests a possible trapping at the meteorological equator near 7°N (Gill 1980). Although of weaker magnitude than the AEW, the ER and the MRG waves seem to play a role in building the anomalous southerlies and northerlies, with the MRG and AEW in phase at the longitude of the event, and a possible role of ER further to the east.

The quantitative contribution of each wave to the development of the anomalous southerlies and northerlies is further analysed with Fig. 8, which shows zonal profiles of the meridional mass transport and contributions averaged over the 5–15°N band. These allow for a clearer view of the different scales involved in the event.

The ER wave (blue curve in Fig. 8) has a zonal wavelength of about 60° and propagates westward at ~4 m s^{-1}. Its positive phase impacts Eastern Africa during the last 10 days of August (in agreement with Fig. 6). It drives a mean southerly flow, up to 1.5 ms^{-1}, that may largely contribute to the formation of the wide and long wet spell over the Eastern Sahel. For instance, on 27th August (Fig. 8a) the ER contributes more than the AEW (green curve) to southerlies east of 20°E.

The MRG wave (red curve in Fig. 8) has a zonal wavelength of about 40° and propagates westward at ~6.4 ms^{-1}. Although the MRG wave magnitude is weak (~1 ms^{-1}) as compared with AEWs (~4 ms^{-1}), its role in the occurrence of the extreme event of Ouagadougou cannot be neglected. Indeed the two waves (AEW and MRG) propagating at different speeds become in-phase on 30th August (Fig. 8d), which probably helped the intensification of the ridge R1.

The above wave decomposition (Fig. 7 and 8) omits zonal wavelengths shorter than 2000 km, so it cannot explain the whole structure of the present extreme event. For instance on 28th August AEW and ER (green and blue curves in Fig. 8b) explain only one half of the intense southerly burst (black curve) occurring around 20°E at a scale less than 10°. It is suggested that small-scale processes such as convection may explain this structure associated with the genesis of the vortex T1 (Hall *et al.* 2006, see section 5). It is also to be noticed that the arrival of Kelvin wave K2 over the Sahel cannot be seen on the meridional component but it is consistent with the westerly anomaly found ahead of the trough T2 (Fig. 4b).

The time evolution from 1st August to 10th September of the vertical profile of meridional wind provided by the Abidjan soundings is shown in Fig. 9a. It corresponds to the location where the strong southerly burst reaches its maximum on 30th August. At low levels up to 850 hPa the flow is always northward corresponding to the monsoon and its meridional component reaches 6-7 ms^{-1}. Above, in the 850-500 hPa layer, a large oscillation (with fluctuations between -6 and 10 ms^{-1}) occurs with a maximum amplitude near 700 hPa. Consequently, the southerly burst is mainly due to the deepening of the monsoon layer up to 500 hPa (in particular to the contribution of the 600-750 hPa layer). Figure 9b provides a similar time-height series for ERA-I meridional wind averaged in the [0 – 10°N] band. It shows that the reanalysis captures a similar signal over a larger band, which lends confidence to the previous wave-analysis results. Other short-period wave trains are detected above 500 hPa in Fig. 9. Further studies will be needed to explain them and their role. A first wave train in the 500-300 hPa layer may contribute to the intensification and deepening of the monsoon flow. The second one at upper levels may be connected to the modulation of the TEJ through the convective activity of the ITCZ (Nicholson *et al.* 2007).

5. **From synoptic to convective scales**

a. The breaking signature of the AEW

The longitude-time diagram of the TRMM rainfall and the ARPEGE 700-hPa meridional wind (Fig. 10a) illustrates the passage at Ouagadougou of the troughs T1 (30th August, 00 UTC) and T2 (1st September, 18 UTC). Between T1 and T2, the ridge R1 is associated with a strong southerly flow whose strength is maximum on 30th August between 12 and 00 UTC as already noted in Fig. 4. Confirming Fig. 4, the latitude-time diagram (Fig. 10b) shows that the extreme event of Ouagadougou (MCS1) occurred about 12 h before the passage of T2, in the northerly flow (Fig. 10a), and to the south of the intense AEJ core (Fig. 10b). The AEW breaking – defined by Cornforth *et al.* (2017) as a very steep north-south oriented curvature of the wave streamlines (Fig. 4c) – reaches Ouagadougou on 31st August, 12 UTC (Fig. 10b). The breaking is so strong that a north-westerly flow at 700 hPa (i.e. overturning) is observed during more than one day south of Ouagadougou (from 31th August 12 UTC to 2nd September at 00 UTC). After the passage of T2, convection is suppressed during two days before the passage of another MCS (labelled MCS2 in Fig. 10b) of weaker intensity at the Ouagadougou meridian and linked to AEW3 with an AEJ core located more to the north (16 – 20°N). This last trough T3 of the AEW train will be the strongest and will be responsible of the genesis of the hurricane Fred (Fig. 5).

Vertical cross-sections of the relative vorticity field (not shown) and the barotropic structure of the winds (Fig. 4 and 9) indicate that the Ouagadougou extreme event corresponds to a deep vortex (AEW2 through T2), which is almost vertically oriented between the surface and 300 hPa, and maximum in the 600-500 hPa layer. To better track this vortex we use the barotropic component of the low-level circulation, being the flow averaged in the 950-600 hPa layer, and analyse the corresponding streamlines, vorticity and wind intensity (Fig. 11). This "barotropic" diagnostic allows an easier detection of strong AEWs. On 29th August , in the lee of AEW1, the initiation of AEW2 over Lake Chad occurs simultaneously with the combination of the AEJ core and the strong southerly flow (Fig. 11a). During 24 hours, AEW2 stays at the same location (2° NW of Lake Chad) and intensifies. It further evolves into a strong closed circulation isolated from AEW1 (Fig. 11b and c), and propagates westwards (8.2 m s^{-1}) until it reaches the Atlantic on 3rd September, 12 UTC (Fig. 11d). The vortex size is small, and its intensity of more than 20×10^{-5} s^{-1} (red colour in Fig. 11), is maximum during the Ouagadougou event (Fig. 11c). When reaching Fouta Djalon (10°W, 10°N, Fig. 11d), the meso-vortex becomes weaker (~10 $\times 10^{-5}$ s^{-1}) but wider.

It is to be noticed that this scenario is reproduced for AEW3 (not shown), which is initiated and intensified in the lee of AEW2 on 3rd September at 00 UTC (see red circle in Fig. 11d for its location), but at a more northern latitude (16°N, 1°E). During 36 hours it intensifies while slowly moving westwards (4.2 ms^{-1}) with the help of a strong ridge as for the previous AEW2 scenario. Then it follows a south-westward trajectory and accelerates (13 ms^{-1}) until it reaches the coast on 6th Sept at 12 UTC and where it initiates hurricane Fred.

b. Coupling between the vortex and the convection

To analyse the link between the organized convection and the vortex signature of the Ougadougou event, Figures 12a to d show the PCT parameter for a selection of four of the 18 AMSRE, SSMI and TRMM satellite imagery snapshots acquired in the vicinity of the vortex. It corresponds to the sampling of the extreme event of Ouagadougou MCS1 tracked between 31st August at 1733 UTC and 1st September at 1328 UTC. The location of the "barotropic vortex" AEW2 as detected in Fig. 11 is indicated by the black circle. Whereas the IR Meteosat Images show a large almost circular cloud shield capping MCS1 (not shown), the PCT parameter allows the identification of narrower convective elements (red/black shading) surrounded by widespread stratiform elements (green shading). The second row of Fig. 12 (e to h) provides the corresponding mean wind vector in the 950-600 hPa layer and accumulated rain over 1 hr.

On 31th August, the snapshot at 1733 UTC (Fig. 12a) reveals the structure of a squall-line (SL) located ahead of the vortex centre of T2. Figure 12e indicates that at 18 UTC this SL is about 2° west of the vortex, on the southern flank of the AEJ core (solid contour). Six hours later, the narrow arc-shaped band of the SL convective element (black-red shading in Fig. 12b) is still identified, but now embedded in a widespread area of moderate-to-weak precipitation (yellow to green) as depicted by the snapshot at 0103 UTC. At that time, Ouagadougou (white dot in Fig. 12b) is at the western edge of the approaching westward-moving SL and the main precipitation area in the south-west sector of the vortex still at a distance of 2° (Fig. 12f). At 06 UTC the system appears as a large (4° diameter) "comma" structure (Fig. 12c, g) with the heaviest convective rains just above Ouagadougo, in the south-west sector of the vortex at a 2° radial distance. To the north the SL is still active ahead the AEJ core reaching its maximum intensity (Fig. 12c). At 12 UTC the convective vortex is slowly decreasing. The snapshot at 1330 UTC (Fig. 12d) exhibits a large area of moderate precipitation around Ouagadougou, whereas the convective part is over northern Ghana about 3° south of the vortex centre (Fig. 12h), consistent with the southward track of the MCS1 at the end of its life cycle. This scenario is consistent with the observed rain record described in section 3a and in

Fig. 1a. The Ouagadougou rainfall peak between 7-8 UTC (97 mm) corresponds to the slow passage of the intense convective elements seen in Fig. 12c (red spots).

An analysis of available SYNOP observations at Ouagadougou (not shown, Chapelon personal communication) showed that the convective system MCS1 was not associated with surface gusts, nor with convective cold pools contrary to the typical Sahelian SLs. Indeed the mid-levels were very humid (wet potential temperature θ'_w = 23°C) as compared with surface temperature 26°C, which prevents strong rain evaporation and cold pool formation as the main driver of the MCS organisation. In contrast with the SL type, the extreme rainfall is associated with a strong meso-vortex, about 2° downshear of its centre, in a region of strong northerly wind. Due to the AEJ, the shear is westward. Such an organisation of convection resembles the conceptual model proposed by Raymond and Jiang (1990) where the diabatic effects of moist convection in a sheared environment can contribute to force vertical motion. A key factor in obtaining this organisation is the pre-existence of a moist anomaly over the northern Sahel. This ensures that northerly wind ahead of the vortex (or of the AEW trough) brings moister air where the ageostrophic forced circulation induces ascent, which supports convection. On the contrary for a Sahelian SL, as northerlies bring drier air, convection is maintained by the cold pool propagation generated by rain evaporation in the dry air. The companion paper will further study the interactions between the mesoscale vortex and the convection using convection-permitting simulations.

6. Summary and conclusion

This first paper presents a multi-scale analysis of an extreme rain event that occurred over Burkina Faso on 1st September 2009, with a record for the Western Sahel of 263 mm observed at

Ouagadougou. Through THORPEX-Africa, daily rain-gauge data from a network of 579 stations over West Africa were collected over a 20-day period centred on 1st September. This dataset is very valuable for the present study and for further ones, in particular to assess the skills of NWP systems to forecast such HIW events.

This case study occurred during a wet spell phase that crossed the whole Sahel in the last 10 days of August and the first 10 days of September, marked by heavy precipitation leading to floods in many Sahelian countries (e.g., Niger, Senegal, Mauritania, Gambia). Rain gauge data confirm the intense rainfall activity over West Africa during this period - also associated with the occurrence of a large number of strong events (22) with daily recorded precipitation above 100 mm - producing much more precipitation than the available water vapour typically stored in the atmospheric column (PW_{max} ~65 mm). Although, the Ouagadougou precipitation record is the most extreme, it is not isolated. When compared with rain gauge data, TRMM estimates capture quite well the Ouagadougou extreme event and its trajectory over Burkina Faso. Observed local maxima are, however, underestimated by a factor of two, possibly due to the lower resolution of the TRMM estimate.

The 2009 wet season appears as a wet dipole year over the Sahel as defined by Nicholson (2009). Rainfall is weaker in June and July corresponding to a late onset, but the deficit is made up during the very active period of August-September. It is to be noticed that the footprint of the Ouagadougou extreme event is detected at the seasonal scale, as well as for intense events over Senegal, South Mauritania and Niger.

The SST anomaly patterns in July-August 2009 of the Atlantic cold tongue, the Tropical Atlantic Dipole and the Mediterranean Sea are favourable factors for the WAM northward penetration, and consistent with the classification of 2009 as a Dipole wet year. On the contrary, the impact of El Niño, Indian Ocean warming and negative NAO on the WAM are unclear at this point. Nevertheless the Atlantic warm anomaly in the northern hemisphere due to the warm phase of the Atlantic Multi-decadal Oscillation appears to favour Sahel precipitation during El Niño as suggested by Rodriguez-Fonseca et al. (2011).

At synoptic scales the Ouagadougou extreme event was associated with a well pronounced “breaking” AEW, whose six favourable factors have been identified by forecasters in several case studies and proposed in the synoptic chapter 2 of the “West African Forecaster's Handbook” (Cornforth *et al.* 2017). The present study confirms four of them:

(1) *A pre-existing significant monsoon flow penetration over the eastern Sahel*, resulting in a large-scale wet spell (positive anomaly of PW, see Fig. 5b) over the Eastern Sahel, that propagates westward.

(2) *A train of AEWs* (see Fig. 4 and 5a). The trough of the second AEW appears to be reinforced by the first one. A strong ridge develops between them, with dryer conditions, which slows down the propagation of the second trough and allows its intensification. This is consistent with the upstream propagation of AEW energy discussed in Diaz and Aiyyer (2013).

(3) *An intense AEJ core* (see Fig. 4 and 5a), associated with the growing second trough.

(4) *Interaction with a deep and intense monsoon flow from the equatorial band.* This monsoon burst can be detected by the southwesterly wind between the surface and 600 hPa, reaching more than 7.5 m s^{-1} (see Fig. 7).

The last two factors identified by Cornforth *et al.* (2017) (*i.e.* (5) *Coupling with midlatitudes* and (6) *Intense convective activity to the south of the AEJ*) need further analysis to assess their respective roles for this extreme event.

The present study further suggests additional specific features that may have played a crucial role in favouring the occurrence of this extreme event. At a regional scale the passage of a Kelvin wave (Fig. 6) over Africa before the event may have generated favourable conditions for convection (large-scale divergence at 200 hPa, Fig. 6a), southerly burst (Fig. 5c) and AEW activity. It is supported by Ventrice et al. (2011) who showed that MJO phase 3 is favourable to AEW activity over West Africa and can help in initiating convective systems. The composite study of Ventrice and Thorncroft (2013) concluded that AEW activity increases during and after the passage of the convectively active phase of strong convectively-coupled Kelvin waves. This mechanism seems to be at work for the Ouagadougou extreme event (Fig. 6). It is also to be noticed that in both studies with a similar Kelvin wave scenario, a hurricane resulted (Alberto 2000 and Fred 2009).

In the present study, equatorial Rossby waves appear as an important supplementary ingredient whose envelop corresponds to the strong convective activity that crossed Africa westwards during the last 10 days of August. The equatorial Rossby wave passage is associated with a deepening and enhancement of the southerly component of the monsoon flow mainly over the central and eastern Sahel (Fig. 7d ,e , f), which may contribute to generate the large-scale wet spell (factor (1) above). At a finer scale, trapped westward-propagating MRG waves have been detected in the 5 – 10°N band allowing a modulation of the mean meridional wind in the surface to 600 hPa layer (factor (4) above). Combined with AEW1, MRG waves helped to reinforce the monsoon burst and the associated ridge behind the AEW1 trough on 30th August resulting in the amplification of the AEW2 (factor (2) above).

The precipitating system itself does not resemble a fast moving squall-line which is the dominant type of MCS observed over the Sahel. It corresponds to a moist, slowly-propagating vortex which allows the accumulation of substantial rainfall, while no surface gust winds nor convective cold pools were observed at the surface. The main precipitation area is located about 2° downshear (westward due to the AEJ) of the centre of this strong mesovortex, in a region of strong northerly wind. In a companion paper we will analyse the physical mechanisms involved in the development of the moist vortex associated with this extreme rain event at a small-scale, by using the computation of budgets of heat, moisture and vorticity from a convection-permitting simulation.

This study suggests that this extreme rainfall event results from the combination of several favourable ingredients arising at different scales such as SST patterns, equatorial waves including MJO, Kelvin, ER, MRG and an AEW train, as well as a pre-existing large-scale wet spell. Further studies are necessary to confirm the relative importance of these ingredients and of their combination based on other case studies of extreme events and on statistical studies. If confirmed, these results may increase our skills in anticipating them, especially if the NWP and climate models are able to represent and forecast those favourable ingredients.

Acknowledgments

This work was supported by the WMO THORPEX program. The authors would like to acknowledge the NWHSs of the following West African countries: Benin, Burkina Faso, Cap Verde, Ivory Coast, Gambia, Ghana, Guinea-Bissau, Guinea-Conakry, Mauritania, Nigeria, Senegal and Togo for providing precipitation data. We also thank NCAR for the use of the ncl library, in particular for the analysis of equatorial waves. Francoise Guichard and Philippe Peyrillé have received funding for this research from the NERC/DFID Future Climate For Africa programme under the AMMA-2050 project, grant number NE/ M019950/1. We thank the two anonymous reviewers whose numerous comments and suggestions helped us to improve the text.

Table

Wave type	Propagation	Period T	Zonal wave number k	Zonal wavelength range	Variables from ERA-I
MJO	Eastward	30-96 days	1-5	8 000 – 40 000 km	VP_{200}, OLR, Vm
Kelvin	Eastward	25-30 days	1-14	2 800 – 40 000 km	VP_{200}, OLR, Vm
ER	Westward	9.7-48 days	1-10	4 000 – 40 000 km	VP_{200}, OLR, Vm
MRG	Westward	3-96 days	1-10	4 000 – 40 000 km	V_m
TD-type (AEW)	Westward	2-5 days	6-20	2 000 – 6 600 km	V_m

Table 1: Characteristics of the filters in the space-time spectral domain used to extract main types of Equatorial waves. These filters are similar to those of Roundy and Frank (2004) (see their Fig. 4 for illustration). Depending on the wave type, the filtering is applied to different ERA-I variables: Velocity potential at 200 hPa (VP200), OLR and the meridional mass transport (Vm) defined as the mass-weighted 950-600 hPa layer-averaged meridional wind.

Captions

Figure 1: (a) 2-day accumulated precipitation (mm) over Burkina Faso from 31st August at 06 UTC to 2nd September at 06 UTC as observed (coloured points) and as estimated by TRMM (red isolines). (b) Observed extrema of daily precipitation over West Africa during the 20-day period from 21st August to 10th September. Values above 100 mm/day (red points) are indicated with the date of occurrence, for instance 120/9 means 120 mm observed on 9th September. (c) and (d) Accumulated precipitation (mm) over the same 20-day period as estimated by TRMM and observed, respectively. (e) Accumulated TRMM precipitation (mm) in JAS 2009 and (f) its anomaly (mm) from the 1998-2014 TRMM climatology. The 1° square around Ouagadougou is outlined in

red in all panels, and the Burkina Faso zoom of panel (a) is superposed on all other panels in black or white.

Figure 2: SST anomalies (°K) during July-August 2009 from the Reynolds climatology over the 32-years period (1982-2014).

Figure 3: (a) TRMM precipitation evolution for the year 2009 (mm/day), averaged over a 1° square around Ouagadougou [12 – 13°N; 1 – 2°W] (red square in Fig. 1). Raw daily data are indicated with white bars. The orange shaded area corresponds to the climatological (1998-2013) annual cycle. The 2009 annual cycle is indicated with the dashed black curve and obtained with a 90-day low-pass spectral filter applied on raw precipitation. The intraseasonal scale is emphasized with a solid black curve and obtained with a 10-day low-pass spectral filter. Red curves in Fig. 2a correspond to the accumulated rain (mm) since 1st January for the climatology (solid red line) and the year 2009 (dashed red line). (b) Wavelet analysis of TRMM precipitation averaged over the 1° square around Ouagadougou and 90-day high-pass filtered.

Figure 4: Maps of the horizontal wind vector at 700 hPa stronger than 5 ms^{-1} (left column), and at 925 hPa stronger than 2.5 ms^{-1} (right column). At 700 hPa light pink shading for wind speed above 12 ms^{-1} (left column) outlines the AEJ cores, whereas at 925 hPa anomalies of precipitable water PW are superposed to highlight moister patches (>5mm light gray shading) and dryer paches (<5 mm dark gray one). For all panels, precipitation rate (mm/hr) are marked with colour shading. Data from ERA-I are shown at 06 UTC on 30th August (a,d), 31st August (b, e) and 1st September (c, f). The location of troughs T1, T2 and T3 (red solid lines) and ridge R1 (red dashed line) are marked in all panels.

Figure 5: Longitude-time diagrams between 40°W and 40°E from 20th August to 10th September 2009 for: (a) vorticity (10^{-5} s^{-1}) at 700 hPa, (b) precipitable water anomaly PW (mm) and (c) meridional mass transport (ms^{-1}) defined as the mass-weighted 950-600 hPa layer-averaged meridional wind. Fields are extracted from the ERA-I reanalysis and averaged in the 10 – 18°N band. Zonal wind averaged over the 700-600 hPa layer is superimposed on panel (a) only for strong easterlies to highlight the AEJ intensity (isolines between -15 and -20 ms^{-1} with a 2.5 ms^{-1} interval). Also the trough of each AEW (labelled from T1 to T3) corresponding to the line of maximum vorticity is superposed on all panels (dotted black or yellow lines). The passage of the wet spell corresponding to a band of positive PW anomaly (b), is outlined by the blue lines on all panels. The white dot indicates the location of Ouagadougou event. The black and blue heavy dashed arrows superposed on panel (c) correspond to the track of the Kelvin [K2] and Rossby [ER] waves, respectively detected ion Fig. 6.

Figure 6: Longitude-time diagrams from 1st August to 10th September of daily anomalies of (a) velocity potential (10^6 m^2s^{-1}) at 200 hPa and (b) OLR (W m^{-2}). Anomalies are averaged in the 5°N – 15°N band and are relative to the ERA-I and OLR climatologies over the 1979-2014 period. Favourable phases for convection are superimposed for MJO (black dash–dot isolines), Kelvin (black dashes) and Equatorial Rossby waves (blue dashes). Isolines are plotted at -1.5, -3 and -6 10^6 m^2s^{-1} for (a), and at -5, -10 and -15 W m^{-2} for (b). The 3 black circles mark the the location of the trough T2 on 30th, 31st August and 1st September. Africa is delimited by vertical dashed lines (between 15°W and 45°E).

Figure 7: Daily mean maps of the meridional mass transport (colour, in m s^{-1}) defined as the mass-weighted 950-600 hPa layer-averaged meridional wind, with the contributions (isolines, 0.5 m s^{-1} interval, northerlies dashed) of the AEW, ER and MRG waves (left, middle and right columns,

respectively) on 30th 31st August and 1st September (upper, middle and bottom rows, respectively). The black triangle and cross correspond to the Abidjan and Ouagadougou locations, respectively. The location of troughs T1 and T2 (red solid lines) and ridge R1 (red dashed line) have been superposed on all panels.

Figure 8: Zonal distribution of the meridional mass transport (m s^{-1}) defined as the mass-weighted 950-600 hPa layer-averaged meridional wind, at 00 UTC averaged in the 5 – 15°N band (black curve) and the corresponding contributions of the ER (blue), MRG (red) and AEW (green) waves. Black arrows represent the propagation of the AEW troughs T_1 and T_2, whereas blue and red dashed arrows track the maximum of southerly wind associated with ER and MRG waves, respectively. The black dashed line represents the total contribution of ER, MRG and AEW waves. The panel series show the evolution from 27th August to 1st September 2009 at a daily frequency.

Figure 9: Evolution between the 1st August and the 10th September of the vertical profile of meridional wind (m s^{-1}) (a) observed twice a day at Abidjan [5.18°N, 4°W], and (b) averaged in the [0° – 10°N] band at the same longitude (4°W) from ERA-I reanalysis.

Figure 10: (a) Longitude-time and (b) latitude-time diagrams of 3-hour accumulated TRMM rainfall (colour in mm h^{-1}) from 30th August to 4th September. The meridional wind at 700 hPa (isoline in ms^{-1}) of the ARPEGE reanalysis is superposed in panel (a), with northerlies dashed. Horizontal wind vector at 700 hPa is added to panel (b) with isolines of intensity at 15 and 20 ms^{-1} to outline the AEJ core. Fields are averaged in the [10 – 14°N] latitude-band for (a) and in the [2.5°W – 0.5°W] longitude-band for (b) surrounding Ouagadougou. The longitude and latitude of Ouagadougou are indicated by vertical and horizontal dashed lines on panels (a) and (b), respectively. Troughs T1 and T2, and ridge R2 are indicated and labelled in red on both figures.

Figure 11: Tracking of the vortex associated with AEW2 for the ARPEGE reanalysis as visualized by the streamlines (blue) for the mean flow mass-weighted averaged in the 950-600 hPa layer, with mean horizontal wind speed (back isolines above 7.5 ms^{-1}) and relative vorticity (colour, 10^{-5} s^{-1}). The analysis is performed at a 36 hour interval between the 29th August at 06 UTC and 3rd September at 00 UTC. Crosses indicate the location of the vortex centre every 3 hours, whereas the red arrows show the progression of the AEW1 and AEW2 troughs. The red circle on panel (d) corresponds to the first detection of T3.

Figure 12: Upper row (a to d): satellite snapshots of the Polarized Corrected Temperature (PCT in °K) in the vortex vicinity indicated by the black circle (times are UTC). Light precipitation (1-3 mm/h) is delimited by PCT > 255 K (green shading), while convective precipitation (10-12 mm/h) correspond to PCT < 225 K (warm shading). The white dot corresponds to the Ouagadougou location. The black circle indicates the location of the mean vortex centre as detected by the ARPEGE reanalysis.

Lower row (e to h): one-day evolution at a 6 hour frequency from 31st September at 18 UTC of the GSMAP accumulated rain over 1 hr (colour in mm) and of the mean wind vector field over the 950-600 hPa layer as analysed by ARPEGE. Maps are drawn relative to the mean vortex centre in a 10° square domain. Heavy black contours outline wind speed higher than 12.5 ms^{-1}.

References

Arndt D. S., M. O. Baringer and M. R. Johnson: State of the Climate in 2009. Bulletin of the American Meteorological Society. Volume 91, Issue 7 (July 2010) pp. s1-s222 doi: http://dx.doi.org/10.1175/BAMS-91-7-StateoftheClimate

Bader J, Latif M. 2003. The impact of decadal-scale Indian Ocean sea surface temperature anomalies on Sahelian rainfall and the North Atlantic Oscillation. *Geophys. Res. Lett.* **30**(22), 2169, doi:10.1029/2003GL018426.

Barthe C., N. Asencio, J.-P. Lafore, M. Chong and B. Campistron, 2010: Cloud-resolving model simulation of the 25-27 July 2006 convective period over Niamey: comparison with radar data and other observations. *Q. J. Roy. Meteorol. Soc.*, 190-208. DOI: 10.1002/qj.539

Benson C, Clay EJ. 1998. The impact of drought on sub-Saharan economies. *World Bank Technical Paper*, vol. 401. World Bank:Washington DC.

Beucher F., J-P. Lafore, F. Karbou and R. Roca, 2013: High-resolution prediction of a major convective period over West Africa . *Q. J. R. Meteorol. Soc.* 139. DOI:10.1002/qj.2225

Birch, C. E., D. J. Parker, A. O'Leary, J. H. Marsham, C. M. Taylor, P. P. Harris, and G. M. S. Lister (2012), Impact of soil moisture and convectively generated waves on the initiation of a West African mesoscale convective system, *Q. J. R. Meteorol. Soc.*, doi:10.1002/qj.2062

Caniaux G, Giordani H, Redelsperger JL, Guichard F, Key E, Wade M. 2011.Coupling between the Atlantic cold tongue and the West African monsoon in boreal spring and summer. *J. Geophys. Res.* **116**(C04003), doi:10.1029/2010JC006570.

Chalon J-P, G. Gaubert, J-P. Lafore and F. Roux 1988: The West African Squall Line Observed on 23 June 1981 during COPT 81: Mesoscale Structure and Transports. *J. Atm. Sci.*, **45**, DOI: http://dx.doi.org/10.1175/1520-0469(1988)045<2744:TWASLO>2.0.CO;2

Chong, M., Amayenc, P., Scialom, G. and Testud, J. 1987 A tropical squall line observed during the COPT81 experiment in West Africa. Part I: Kinematic structure inferred from dual doppler radar data. *Mon. Weather Rev.*, **115,** 670–694

Chong, M. (2010), The 11 August 2006 squall-line system as observed from MIT Doppler radar during the AMMA SOP. Q.J.R. Meteorol. Soc., 136: 209–226. doi: 10.1002/qj.466.

Courtier P, Thépaut J-N, Hollingsworth A. 1994. A strategy for operational implementation of 4D-Var, using an incremental approach. Q. J. R. Meteorol. Soc. **120**: 1367–1387.

Cornforth R., Z. Mumba, D. J. Parker, G. Berry, N. Chapelon, K. Diakaria, M. Diop-Kane, V. Ermert, A. H. Fink, P. Knippertz, J-P. Lafore, A. Laing, S. Lepape, R. Maidment, J. Methven, B. N. Orji, D. Osika, E. Poan, R. Roca, S. Rowell, R. Smith, T. Spengler, C. Taylor, C. Thorncroft, J-C. Vincendon and C. York (2017) Synoptic Systems, in Meteorology of Tropical West Africa: The Forecasters' Handbook (eds D. J. Parker and M. Diop-Kane), John Wiley & Sons, Ltd, Chichester, UK. doi: 10.1002/9781118391297.ch2

Crétat J., Vizy E.K. and Cook K.H. 2015: The relationship between African easterly waves and daily rainfall over West Africa: observations and regional climate simulations. *Clim. Dyn.*, 44: 385. doi:10.1007/s00382-014-2120-x

D'Amato N, Lebel T (1998) On the characteristics of the rainfall events in the Sahel with a view to the analysis of climatic variability. Int J Climatol 18:955–974

Descroix, L., P. Genthon, O. Amogu, J.-L. Rajot, D. Sighomnou, and M. Vauclin, 2012: Change in Sahelian Rivers hydrograph: The case of recent red floods of the Niger River in the Niamey region. Global and Planetary Change, 98–99, 18–30, doi:10.1016/j.gloplacha.2012.07.009.

Dee DP, Uppala SM, Simmons AJ, Berrisford P, Poli P, Kobayashi S, Andrae U, Balmaseda MA, Balsamo G, Bauer P, Bechtold P, Beljaars ACM, van de Berg L, Bidlot J, Bormann N, Delsol C, Dragani R, Fuentes M, Geer AJ, Haimberger L, Healy SB, Hersbach H, H´olm EV, Isaksen L, K°allberg P, K¨ohler M, Matricardi M, McNally AP, Monge-Sanz BM, Morcrette J-J, Park B-K, Peubey C, de Rosnay P, Tavolato C, Th´epaut J-N, Vitart F. 2011. The ERA-Interim reanalysis: Configuration and performance of the data assimilation system. *Q. J. R. Meteorol. Soc.* **125**: 553–597, doi: 10.1002/qj.828.

Diaz ML, Aiyyer A. 2013. Energy dispersion in African easterly waves. J. Atmos. Sci. 70: 130–145, doi: 10.1175/JAS-D-12-019.1.

Diongue, A., J.-P. Lafore, J.-L. Redelsperger, and R. Roca, 2002 : Numerical study of a Sahelian synoptic weather system : initiation and mature stages of convection and its interactions with the large-scale dynamics. *Quart. J. Roy. Meteor. Soc.*, **128**, 1899–1927.

Diongue-Niang, A., H. Dacosta, T. Diedhiou, G. Quantin, G. Panthou, I. Bouzou Moussa, J-P. Vandervaere, A. Diedhiou, B. Fati and L. Descroix, 2017. L'inondation de Dakar en août 2012: Vers une recrudescence des inondations urbaines au Sahel? Submitted to *La Houille Blanche.*

Enfield, D. B., and A. M. Mestas-Nunez, 1999: Multiscale variabilities in global sea surface temperatures and their relationships with tropospheric climate patterns. *J. Climate*, **12**, 2719–2733.

Fink, AH, and Reiner, A. 2003. Spatio-temporal variability of the relation between African Easterly Waves and West African Squall Lines in 1998 and 1999. J. Geophys. Res., 08, 4332. DOI:10.1029/2002JD002816.

Giannini, A., R. Saravanan, and P. Chang (2003), Oceanic forcing of Sahel rainfall on interannual to interdecadal time scale, Science, 302, 1027–1030.

Gill, A. E., 1982: *Atmosphere–Ocean Dynamics.* Academic Press, 666 pp.

Grist JP. 2002. Easterly waves over Africa. Part I. The seasonal cycle and contrasts between wet and dry years. *Monthly Weather Review* **130**: 1337–1359.

Grist JP, Nicholson SE, Barcilon AI. 2002. Easterly waves over West Africa. Part II. Observed and modelled contrasts between wet and dry years. *Monthly Weather Review* **130**: 212–225.

Hall NMJ, Kiladis GN, Thorncroft CD. 2006. Three dimensional structure and dynamics of African easterly waves. Part II: Dynamical modes. *J. Atmos. Sci.* **63**: 2231–2245.

Hopsch S., S. C. Jones and J. H. Keller 2014: Analysis of tropical high impact weather events using TIGGE data. https://ams.confex.com/ams/31Hurr/videogateway.cgi/id/27117?recordingid=27117

Huffman GJ, Adler RF, Bolvin DT, Gu G, Nelkin EJ, Bowman KP, Hong Y, Stocker EF, WolffDB. 2007. The TRMMMultisatellite Precipitation Analysis (TMPA): quasiglobal, multiyear, combined-sensor precipitation estimates at fine scales. *J. Hydrometeorol.* **8**: 3855, DOI: 10.1175/JHM560

Joly M., A. Voldoire, H. Douville, P Terray and JP Royer 2007: African monsoon teleconnections with tropical SSTs: validation and evolution in a set of IPCC4 simulations. Clim Dyn (2007) 29:1–20 DOI 10.1007/s00382-006-0215-8

Karbou F, Rabier F, Lafore J-P, Redelsperger J-L, Bock O. 2010a. Global 4DVar assimilation and forecast experiments using AMSU observations over land. Part II: impacts of assimilating surface-sensitive channels on the African monsoon during AMMA. *Weather and Forecasting* **25**: 20–36.

Karbou F, Gerard E, Rabier F. 2010b. Global 4DVar assimilation and forecast experiments using AMSU observations over land. Part I: impacts of various land surface emissivity parameterizations. *Weather and Forecasting* **25**: 5–19.

Karambiri H. 2009. Brève analyse fréquentielle de la pluie du 1er septembre 2009 à Ouagadougou (Burkina Faso). Note technique 2iE, 4 p.

Kiladis, G. N., M. C. Wheeler, P. T. Haertel, K. H. Straub, and P. E. Roundy (2009), Convectively coupled equatorial waves, Rev. Geophys., 47, RG2003, doi:10.1029/2008RG000266

Kiladis, G. N., C. D. Thorncroft, and N. M. J. Hall, 2006: Three-dimensional structure and dynamics of African easterly waves. Part I : Observations. *J. Atmos. Sci.*, **63**, 2212–2230.

Lafore J-P., N. Chapelon, M. Diop-Kane, B. Gueye, Y. Largeron, S. Lepape, O. Ndiaye, D.J. Parker, E. Poan, R. Roca, R. Roehrig and C. Taylor (2017) Deep Convection, in Meteorology of Tropical West Africa: The Forecasters' Handbook (eds D. J. Parker and M. Diop-Kane), John Wiley & Sons, Ltd, Chichester, UK. doi: 10.1002/9781118391297.ch3

Leroux, S., Hall, N. M. J., 2009. On the relationship between African Easterly Waves and the African Easterly Jet. J. Atmos. Sci. 66, 2303–2316.

Lamb PJ. 1978. Large-scale tropical Atlantic surface circulation patterns associated with Subsaharan weather anomalies. *Tellus* **A30**: 240-251.

Le Barbé, L., T. Level, and D. Tapsoba, 2002: Rainfall Variability in West Africa during the Years 1950–90.J. Clim., 15, 187-202. DOI: http://dx.doi.org/10.1175/1520-0442(2002)015<0187:RVIWAD>2.0.CO;2

Lebel T., and Ali A. 2009. Recent trends in the Central and Western Sahel rainfall regime (1990–2007). *Journal of Hydrology* **375**: 52–64.

Levinson DH, Lawrimore JH. 2008. State of the climate in 2007. *Bulletin of the American Meteorological Society* **89**: 1–179.

Liebmann, B., and C. A. Smith, 1996: Description of a complete (interpolated) outgoing longwave radiation dataset. Bull. Amer. Meteor. Soc., 77, 1275–1277.

Madden, R., and P. Julian, 1971: Detection of a 40-50 day oscillation in the zonal wind in the tropical Pacific. *J. Atmos. Sci.*, **28**, 702–708.

Mathon, V., Laurent, H. & Lebel, T. Mesoscale convective system rainfall in the Sahel. J. Appl. Meteorol. 41, 1081–1092 (2002).

Mohr, K. and E. J. Zipser, 1996: Defining Mesoscale Convective Systems by their 85 GHz Ice-scattering signatures. BAMS, 77(6), 1179-1189.

Nicholson SE. 2001. Climatic and environmental change in Africa during the last two centuries. *Climate Research* **17**: 123–144.

Nicholson SE 2009: On the factors modulating the intensity of the tropical rainbelt over West Africa. *Int. J. Climatol.* **29**: 673–689. DOI: 10.1002/joc

Nicholson SE, Webster PJ. 2007. A physical basis for the interannual variability of rainfall in the Sahel. *Quarterly Journal of the Royal Meteorological Society* **133**: 2065–2084.

Nicholson SE, Barcilon AI, Challa M, Baum J. 2007. Wave activity on the tropical easterly jet. *Journal of the Atmospheric Sciences* **64**: 2756–2763.

Nka, B. N., L. Oudin, H. Karambiri, J. E. Paturel, and P. Ribstein, 2015: Trends in floods in West Africa: analysis based on 11 catchments in the region. Hydrology and Earth System Sciences, 19, 4707–4719, doi:10.5194/hess-19-4707-2015.

Paeth H., A. H. Fink, S. Pohle, F. Keis, H. Mächel and C. Samimi, 2011: Meteorological characteristics and potential causes of the 2007 flood in sub-Saharan Africa. *Int. J. Climatol.* **31**: 1908–1926. DOI: 10.1002/joc.2199

Panthou, G., T. Vischel, T. Lebel, J. Blanchet, G. Quantin, and A. Ali, 2012: Extreme rainfall in West Africa: A regional modeling. Water Resour. Res., 48, W08501, doi:10.1029/2012WR012052.

Panthou G., T. Vischel and T. Lebel 2014: Recent trends in the regime of extreme rainfall in the Central Sahel. *Int. J. Climatol*. **34**: 3998–4006

Parker DE, Folland CK, Ward MN. 1988. Sea surface temperature anomaly patterns and prediction of seasonal rainfall in the Sahel region of Africa. *Nature* **3010**: 483–485.

Peyrillé, P., J.-P. Lafore, and J.-L. Redelsperger, 2007: An idealized two-dimensional framework to study the West African monsoon. Part I: Validation and key controlling factors. *J. Atmos. Sci.*, **64,** 2765-2782

Poan E, R. Roehrig, F. Couvreux, J.-P. Lafore, 2013: West Africa Intraseasonal variability : a Precipitable Water perspective, *Journal of Atmospheric Sciences*, 70, 4, 1035-1052.doi: http://dx.doi.org/10.1175/JAS-D-12-087.1

Raymond D. J. and H. Jiang (1990) A Theory for Long-Lived Mesoscale Convective Systems. *J. Atmos. Sci.*, **47**, No. 24 DOI: http://dx.doi.org/10.1175/1520-0469(1990)047<3067:ATFLLM>2.0.CO;2

Reynolds RW, Rayner NA, Smith TM, Stokes DC, Wang W. 2002. An improved in situ and satellite SST analysis for Climate. *Journal of Climate* **15**: 1609–1625.

Redelsperger, J.-L., and J.-P. Lafore, 1988 : A three-dimensional simulation of a tropical squall line : convective organization and thermodynamic vertical transport. *J. Atmos. Sci.*, 45, 1134-1356.

Redelsperger, J.-L., Diongue, A., Diedhiou, A., Ceron, J.-P., Diop, M., Gueremy, J.-F. and Lafore, J.-P. (2002), Multi-scale description of a Sahelian synoptic weather system representative of the West African monsoon. *Q.J.R. Meteorol. Soc.,* 128: 1229–1257. doi: 10.1256/003590002320373274

Reynolds, R. W., N. A. Rayner, T. M. Smith, D. C. Stokes and W. Wang, 2002: An improved in situ and satellite SST analysis for climate. *J. Climate*, **15**, 1609–1625.

Rodriguez-Fonseca B. *et al*. 2011: Interannual and decadal SST-forced responses of the West African monsoon. *Atmos. Sci. Let.* **12**: 67–74 DOI: 10.1002/asl.308

Roundy, P.E., Frank, W.M., 2004. A climatology of waves in the equatorial region. Journal of the Atmospheric Sciences 61, 2105–2132.

Roux F. 1988: The West African squall line observed on 23 June 1981 during COPT81: Kinemaric and thermodynamics of the convective region. *J. Atmos. Sci*, 45, 406-426.

Rowell, D. P., 2003: The impact of Mediterranean SSTs on the Sahelian rainfall season. *J. Climate,* **16,** 849–862.

Schreck, C., J. Molinari, and A. Aiyyer, 2012: A Global View of Equatorial Waves and Tropical Cyclogenesis. *Mon. Wea. Rev.*, **140**, 774–788, doi: 10.1175/MWR-D-11-00110.1.

Servain J. 1991. Simple climatic indices for the tropical Atlantic Ocean and some applications. *J. Geophys. Res.* **96**(C8):137–146.

Thiaw W. M., 2013: [West Africa] Sidebar 7.3 Africa: The floods of the Sahel in 2012 [in “State of the Climate in 2012”]. *Bull. Amer. Meteor. Soc*., **94** (8), S164–S165.

Tomas RA, Webster PJ. 1997. The role of inertial instability in determining the location and strength of near-equatorial convection. *Q. J. R. Meteorol. Soc.* **123**: 1445–1482.

Schwendike, J. and S. C. Jones, 2010: Convection in an African Easterly Wave over West Africa and the Eastern Atlantic: A model case study of Helene (2006). Quarterly Journal of the Royal Meteorological Society, 136: 364–396.

Sighomnou D, Descroix L, Genthon P, Mahé G, Moussa IB, Gautier E, Mamadou I, Vandervaere JP, Bachir T, Coulibaly B, Rajot JL, Malam-Issa O, Malam-Abdou M, Dessay N, Delaitre E, Faran-Maiga O, Diedhiou A, Panthou G, Vischel T, Yacouba H, Karambiri H, Paturel JE, Diello P, Mougin E, Kergoat L, Hiernaux P. 2013. La crue de 2012 a Niamey: un paroxysme du paradoxe du Sahel? *Sécheresse* **24**: 3–13.

Takayabu, Y. N., 1994: Large-scale cloud disturbances associated with equatorial waves. Part I: Spectral features of the cloud disturbances. *J. Meteor. Soc. Japan*, **72,** 433–448.

Taylor, C.M., D. Belušić, F. Guichard, D. J. Parker, T. Vischel, O. Bock, P. P. Harris, S. Janicot, C. Klein, G. Panthou, 2017 : Frequency of extreme Sahelian storms tripled since 1982 in satellite observations. Nature 544 (7651), 475–478.doi:10.1038/nature22069.

Ushio T, Kubota T, Shige S, Okamoto K, Aonashi K, Inoue T, Takahashi N, Iguchi T, Kachi M, Oki R, Morimoto T, Kawasaki Z. 2009. A Kalman filter approach to the Global Satellite Mapping of Precipitation (GSMaP) from combined passive microwave and infrared radiometric data. *J. Meteorol. Soc. Jpn.* **87A**: 137–151.

Ventrice, M. J., and C. D. Thorncroft, 2013. The Role of Convectively Coupled Atmospheric Kelvin Waves on African Easterly Wave Activity. *Mon. Wea. Rev.* 141, 1910–1924. DOI:10.1175/MWR-D-12-00147.1.

Ventrice, M. J., C. D. Thorncroft, and P. E. Roundy, 2011: The Madden–Julian Oscillation’s Influence on African Easterly Waves and Downstream Tropical Cyclogenesis. *Mon. Wea. Rev.* 141, 1910–1924 DOI: http://dx.doi.org/10.1175/MWR-D-10-05028.1

Vizy, E., and K. Cook, 2009: A mechanism for African monsoon breaks: Mediterranean cold air surges. J. Geophys. Res., 114, D01104, doi:10.1029/2008JD010654.

Westra, S., H. J. Fowler, J. P. Evans, L. V. Alexander, P. Berg, F. Johnson, E. J. Kendon, G. Lenderink, and N. M. Roberts (2014), Future changes to the intensity and frequency of short-duration extreme rainfall, Rev. Geophys., 52, 522–555, doi:10.1002/2014RG000464.

Wheeler M. C., H. H. Hendon, 2004: An All-Season Real-Time Multivariate MJO Index: Development of an Index for Monitoring and Prediction. *MWR*, Vol. 132, No. 8. DOI: http://dx.doi.org/10.1175/1520-0493(2004)132<1917:AARMMI>2.0.CO;2

Wheeler, M., and G. N. Kiladis, 1999: Convectively coupled equatorial waves: Analysis of clouds and temperature in the wavenumber–frequency domain. *J. Atmos. Sci.*, **56,** 374–399.

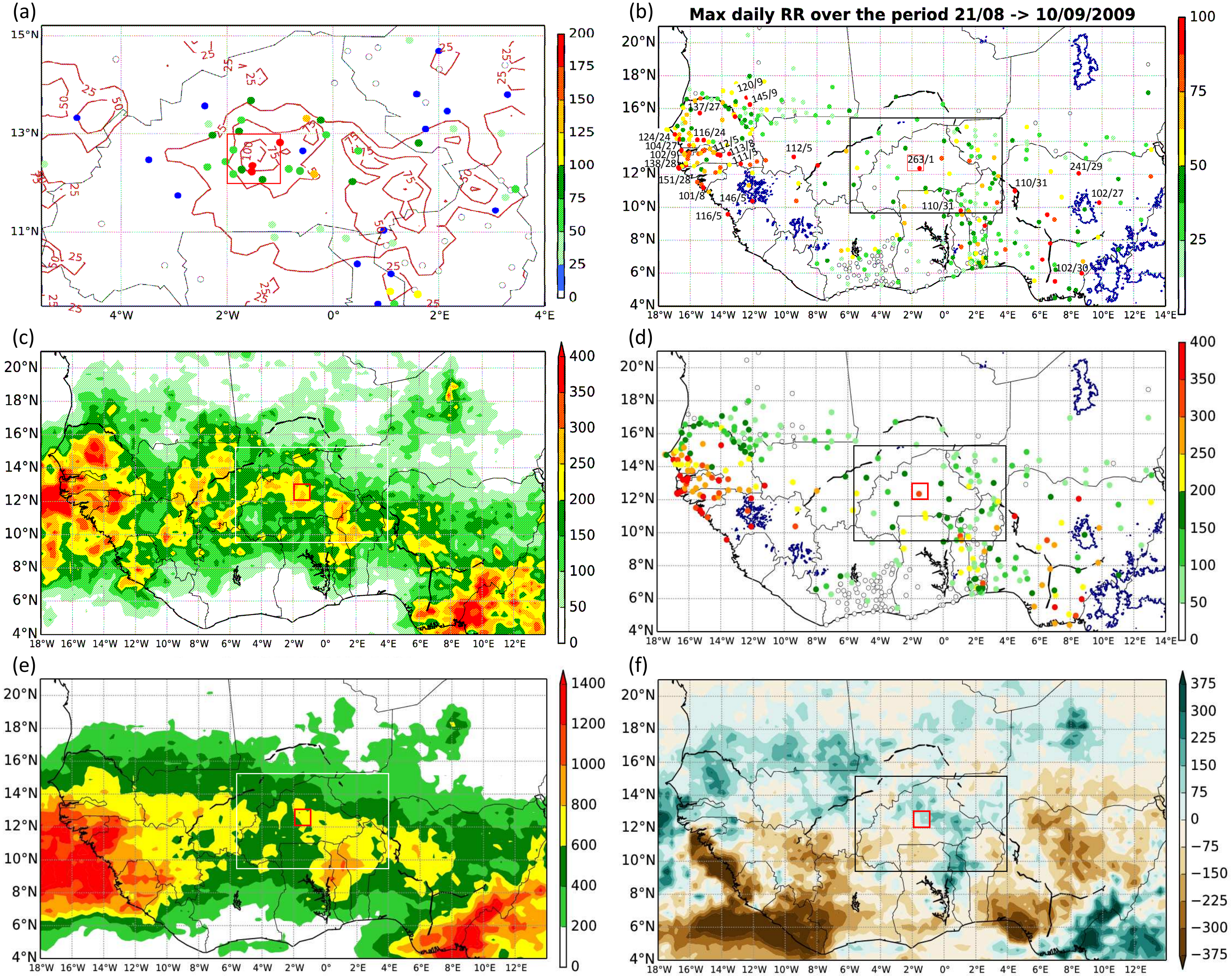

Figure 1:(a) 2-day accumulated precipitation (mm) over Burkina Faso from 31st August at 06 UTC to 2nd September at 06 UTC as observed (coloured points) and as estimated by TRMM (red isolines). (b) Observed extrema of daily precipitation over West Africa during the 20-day period from 21st August to 10th September. Values above 100 mm/day (red points) are indicated with the date of occurrence, for instance 120/9 means 120 mm observed on 9th September. (c) and (d) Accumulated precipitation (mm) over the same 20-day period as estimated by TRMM and observed, respectively. (e) Accumulated TRMM precipitation (mm) in JAS 2009 and (f) its anomaly (mm) from the 1998-2014 TRMM climatology. The 1° square around Ouagadougou is outlined in red in all panels, and the Burkina Faso zoom of panel (a) is superposed on all other panels in black or white.

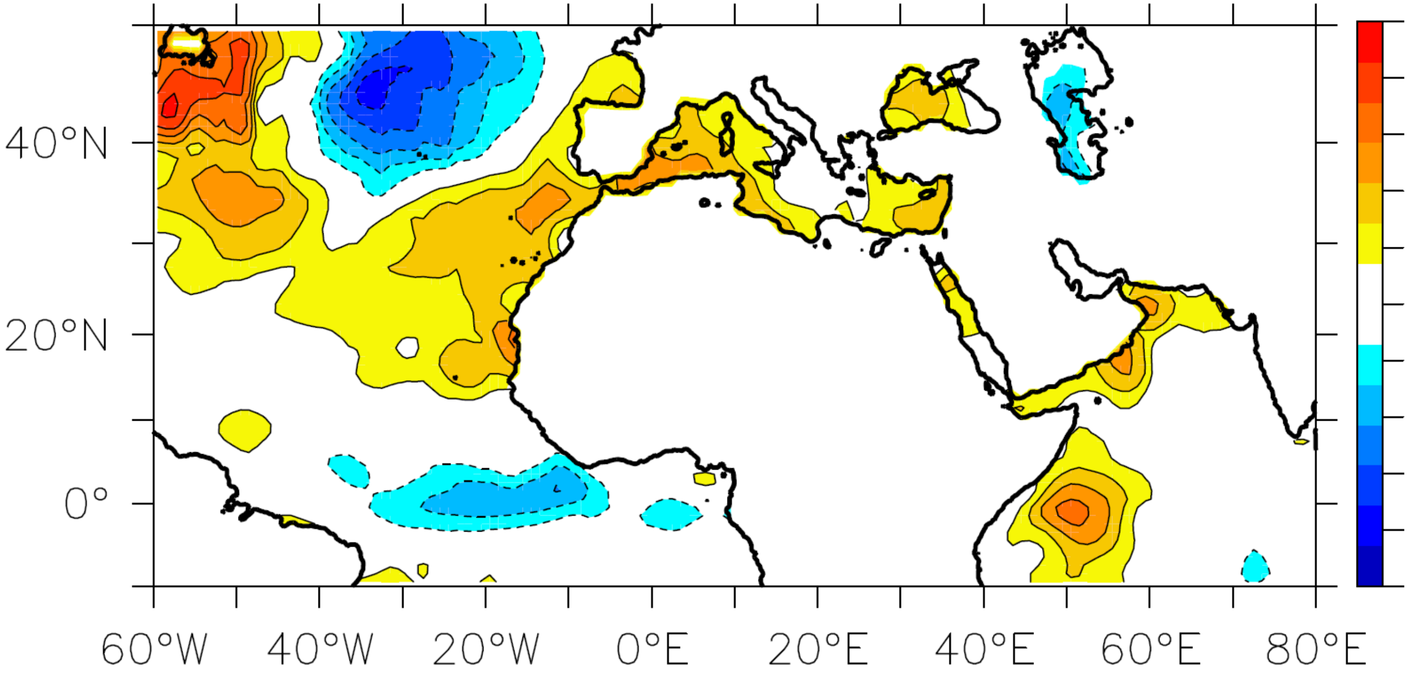

Figure 2: SST anomalies (°K) during July-August 2009 from the Reynolds climatology over the 32-years period (1982-2014).

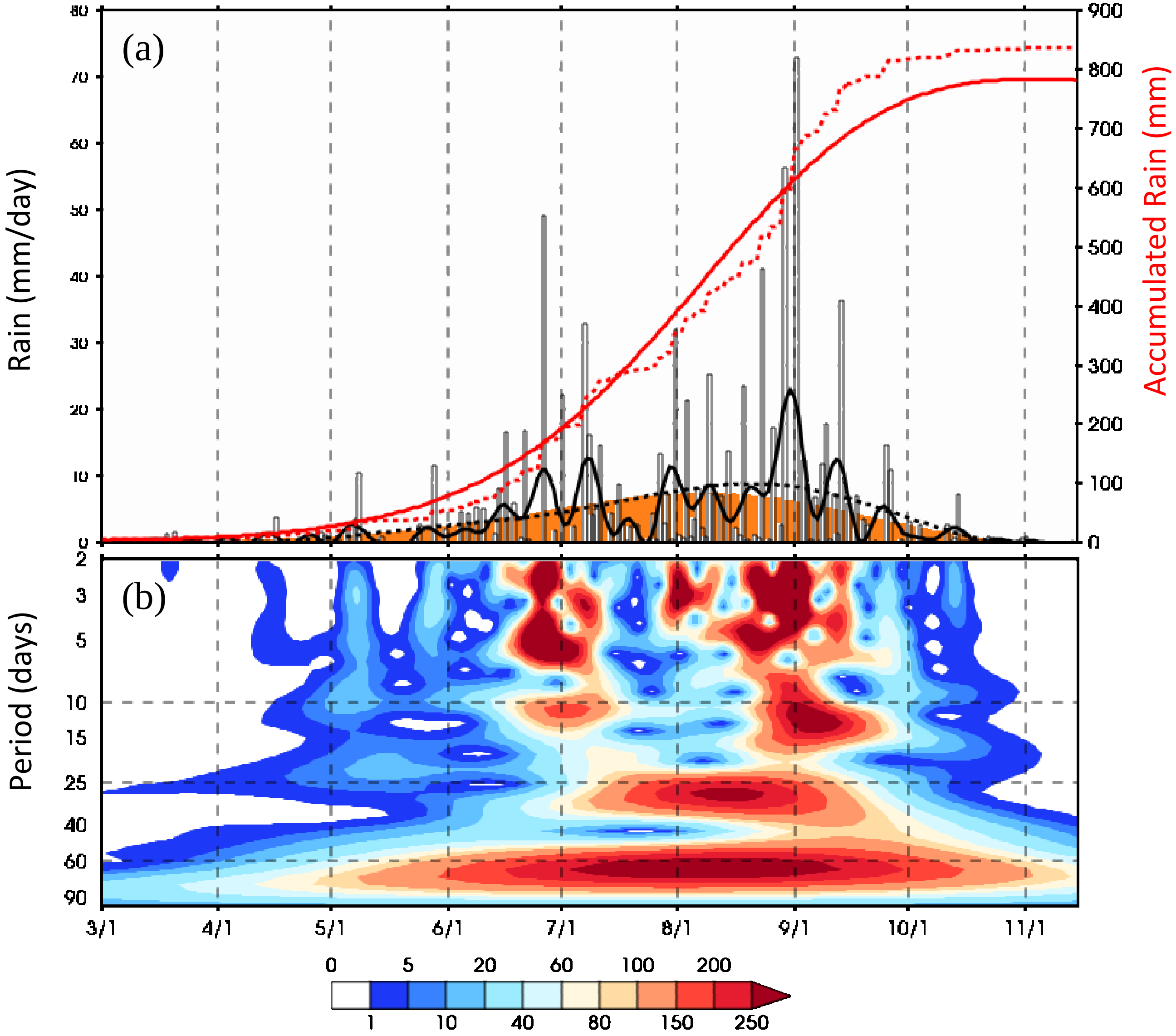

Figure 3:(a) TRMM precipitation evolution for the year 2009 (mm/day), averaged over a 1° square around Ouagadougou [12 – 13°N; 1 – 2°W] (red square in Fig. 1). Raw daily data are indicated with white bars. The orange shaded area corresponds to the climatological (1998-2013) annual cycle. The 2009 annual cycle is indicated with the dashed black curve and obtained with a 90-day low-pass spectral filter applied on raw precipitation. The intraseasonal scale is emphasized with a solid black curve and obtained with a 10-day low-pass spectral filter. Red curves in Fig. 2a correspond to the accumulated rain (mm) since 1st January for the climatology (solid red line) and the year 2009 (dashed red line). (b) Wavelet analysis of TRMM precipitation averaged over the 1° square around Ouagadougou and 90-day high-pass filtered.

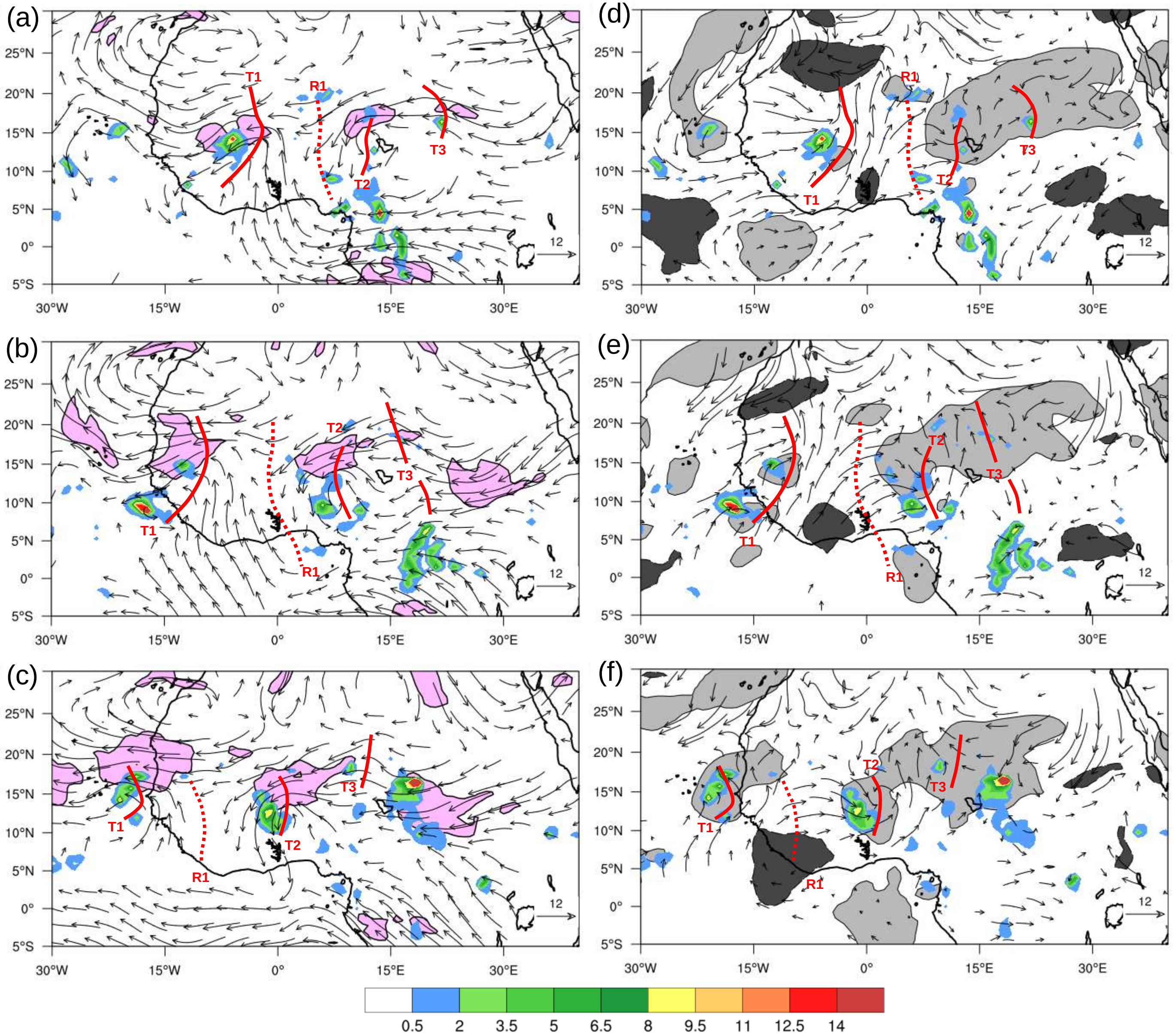

Figure 4: Maps of the horizontal wind vector at 700 hPa stronger than 5 ms^{-1} (left column), and at 925 hPa stronger than 2.5 ms^{-1} (right column). At 700 hPa light pink shading for wind speed above 12 ms^{-1} (left column) outlines the AEJ cores, whereas at 925 hPa anomalies of precipitable water PW are superposed to highlight moister patches (>5mm light gray shading) and dryer paches (<5 mm dark gray one). For all panels, precipitation rate (mm/hr) are marked with colour shading. Data from ERA-I are shown at 06 UTC on 30th August (a,d), 31st August (b, e) and 1st September (c, f). The location of troughs T1, T2 and T3 (red solid lines) and ridge R1 (red dashed line) are marked in all panels.

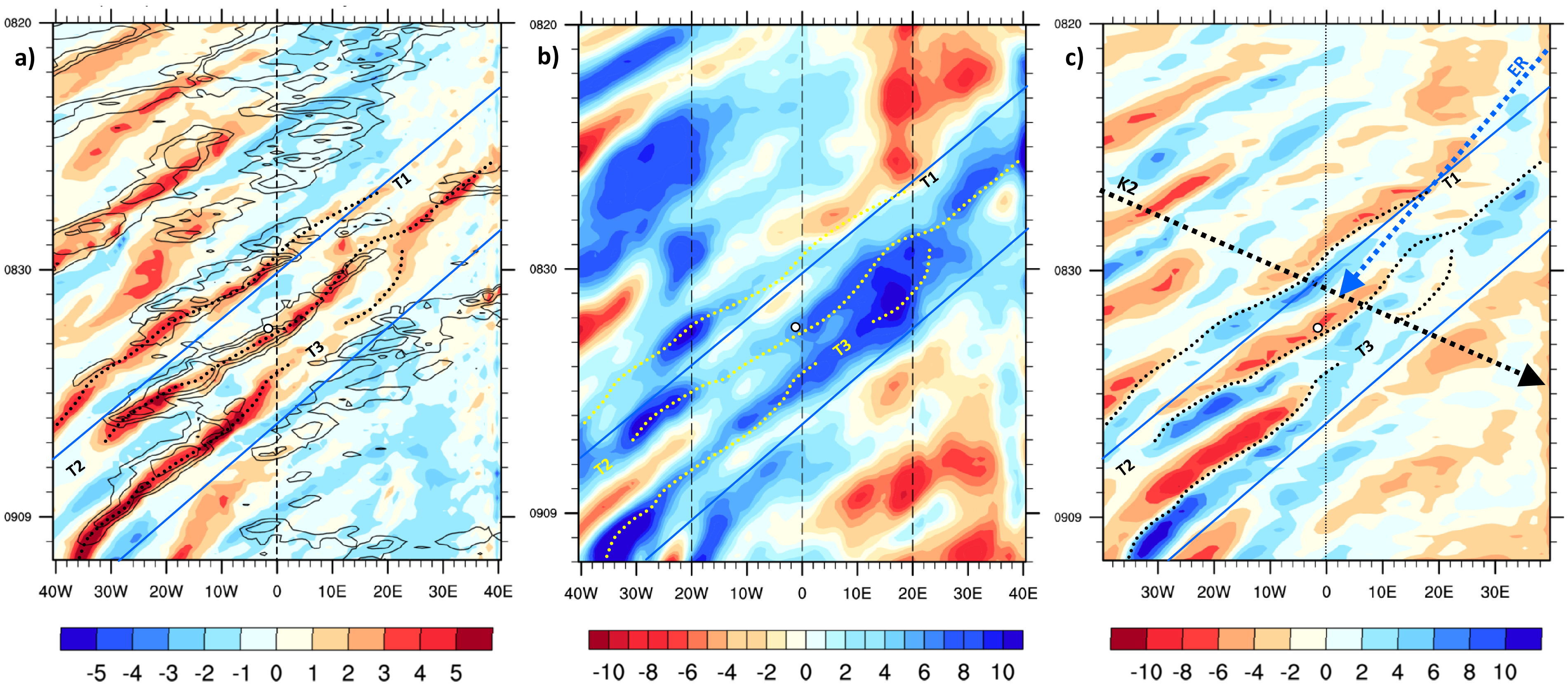

Figure 5: Longitude-time diagrams between 40°W and 40°E from 20th August to 10th September 2009 for: (a) vorticity (10^{-5} s^{-1}) at 700 hPa, (b) precipitable water anomaly PW (mm) and (c) meridional mass transport (ms^{-1}) defined as the mass-weighted 950-600 hPa layer-averaged meridional wind. Fields are extracted from the ERA-I reanalysis and averaged in the 10 – 18°N band. Zonal wind averaged over the 700-600 hPa layer is superimposed on panel (a) only for strong easterlies to highlight the AEJ intensity (isolines between -15 and -20 ms^{-1} with a 2.5 ms^{-1} interval). Also the trough of each AEW (labelled from T1 to T3) corresponding to the line of maximum vorticity is superposed on all panels (dotted black or yellow lines). The passage of the wet spell corresponding to a band of positive PW anomaly (b), is outlined by the blue lines on all panels. The white dot indicates the location of Ouagadougou event. The black and blue heavy dashed arrows superposed on panel (c) correspond to the track of the Kelvin [K2] and Rossby [ER] waves, respectively detected ion Fig. 6.

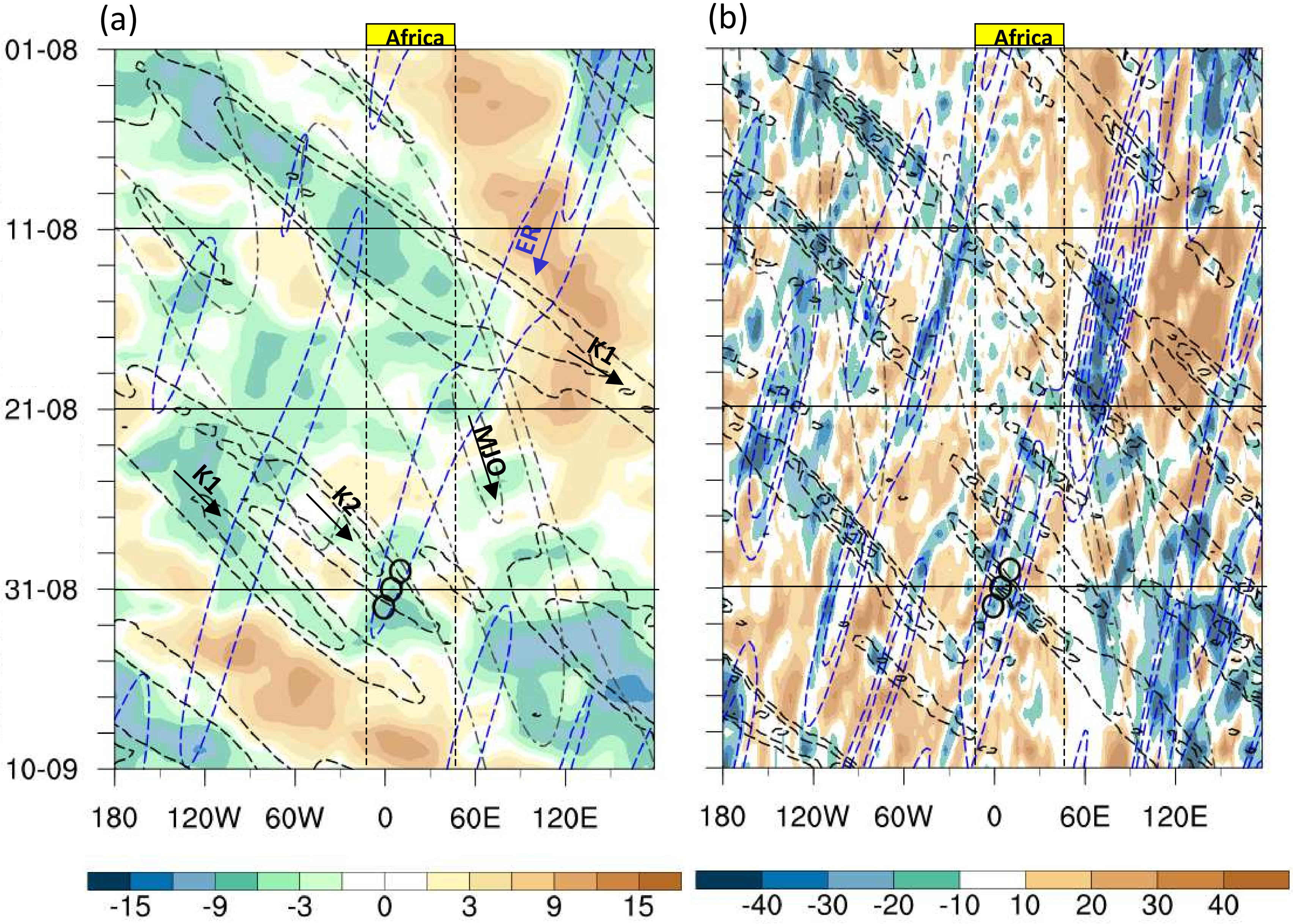

Figure 6: Longitude-time diagrams from 1st August to 10th September of daily anomalies of (a) velocity potential (10^6 m^2s^{-1}) at 200 hPa and (b) OLR (W m^{-2}). Anomalies are averaged in the 5°N – 15°N band and are relative to the ERA-I and OLR climatologies over the 1979-2014 period. Favourable phases for convection are superimposed for MJO (black dash–dot isolines), Kelvin (black dashes) and Equatorial Rossby waves (blue dashes). Isolines are plotted at -1.5, -3 and -6 10^6 m^2s^{-1} for (a), and at -5, -10 and -15 W m^{-2} for (b). The 3 black circles mark the the location of the trough T2 on 30th, 31st August and 1st September. Africa is delimited by vertical dashed lines (between 15°W and 45°E).

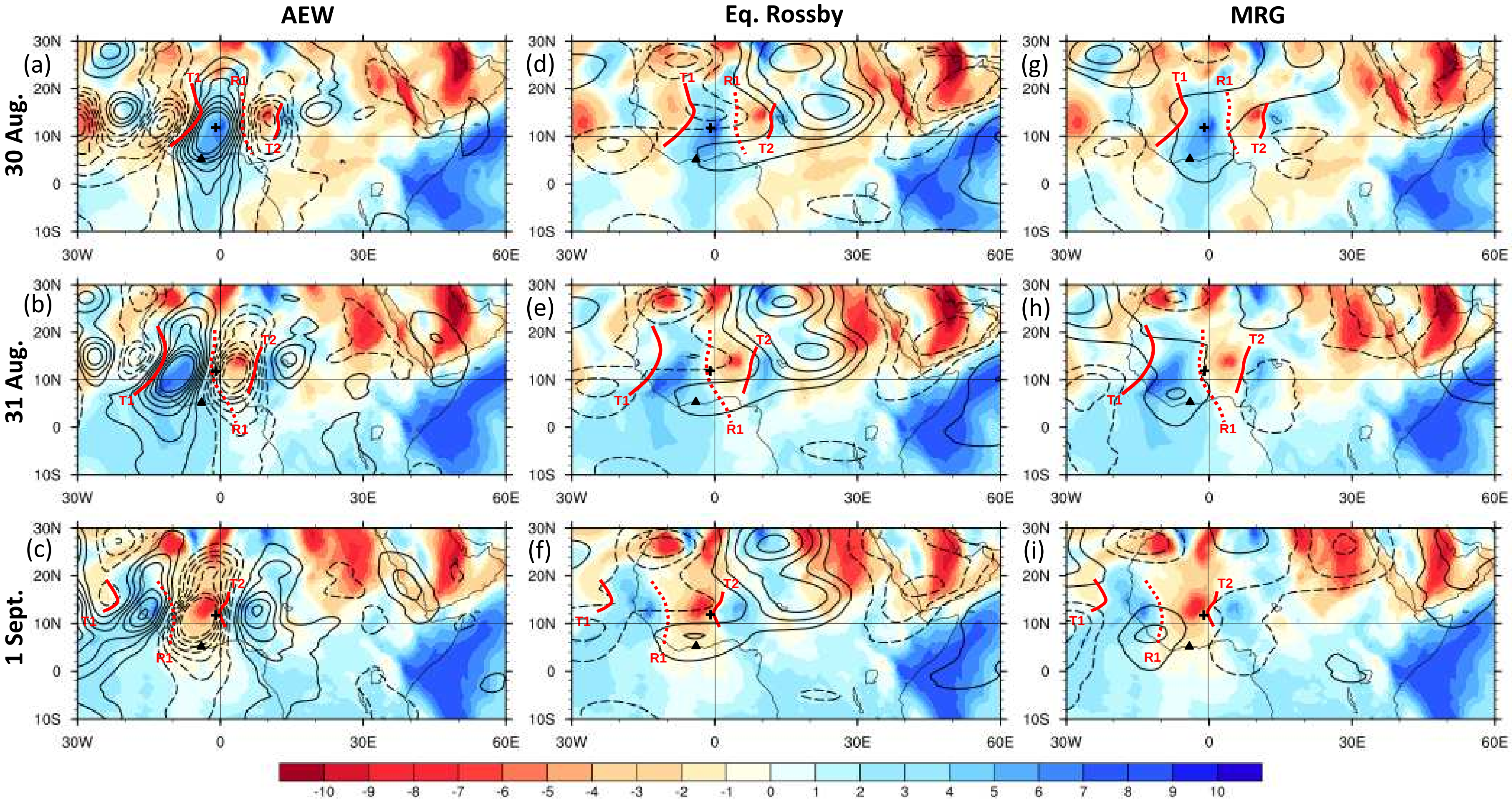

Figure 7: Daily mean maps of the meridional mass transport (colour, in m s^{-1}) defined as the mass-weighted 950-600 hPa layer-averaged meridional wind, with the contributions (isolines, 0.5 m s^{-1} interval, northerlies dashed) of the AEW, ER and MRG waves (left, middle and right columns, respectively) on 30th 31st August and 1st September (upper, middle and bottom rows, respectively). The black triangle and cross correspond to the Abidjan and Ouagadougou locations, respectively. The location of troughs T1 and T2 (red solid lines) and ridge R1 (red dashed line) have been superposed on all panels.

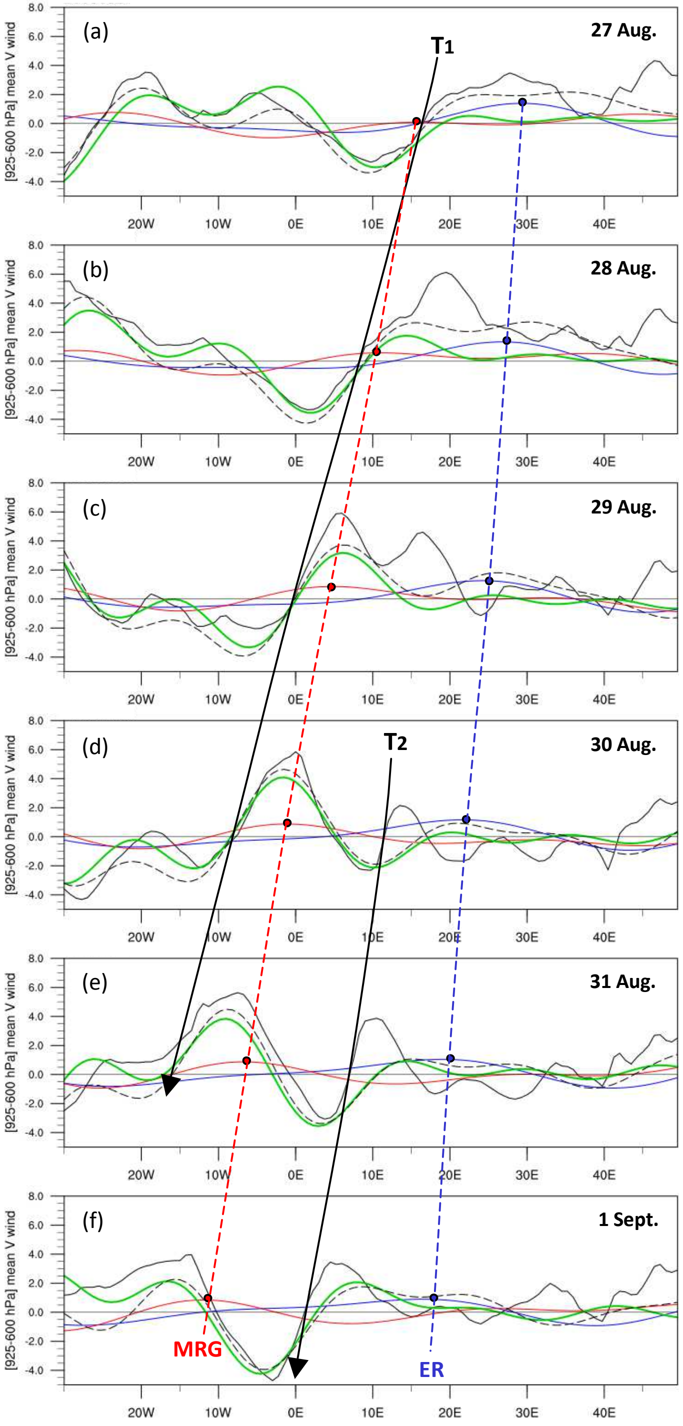

Figure 8: Zonal distribution of the meridional mass transport (m s^{-1}) defined as the mass-weighted 950-600 hPa layer-averaged meridional wind, at 00 UTC averaged in the 5 – 15°N band (black curve) and the corresponding contributions of the ER (blue), MRG (red) and AEW (green) waves. Black arrows represent the propagation of the AEW troughs T_1 and T_2, whereas blue and red dashed arrows track the maximum of southerly wind associated with ER and MRG waves, respectively. The black dashed line represents the total contribution of ER, MRG and AEW waves. The panel series show the evolution from 27th August to 1st September 2009 at a daily frequency.

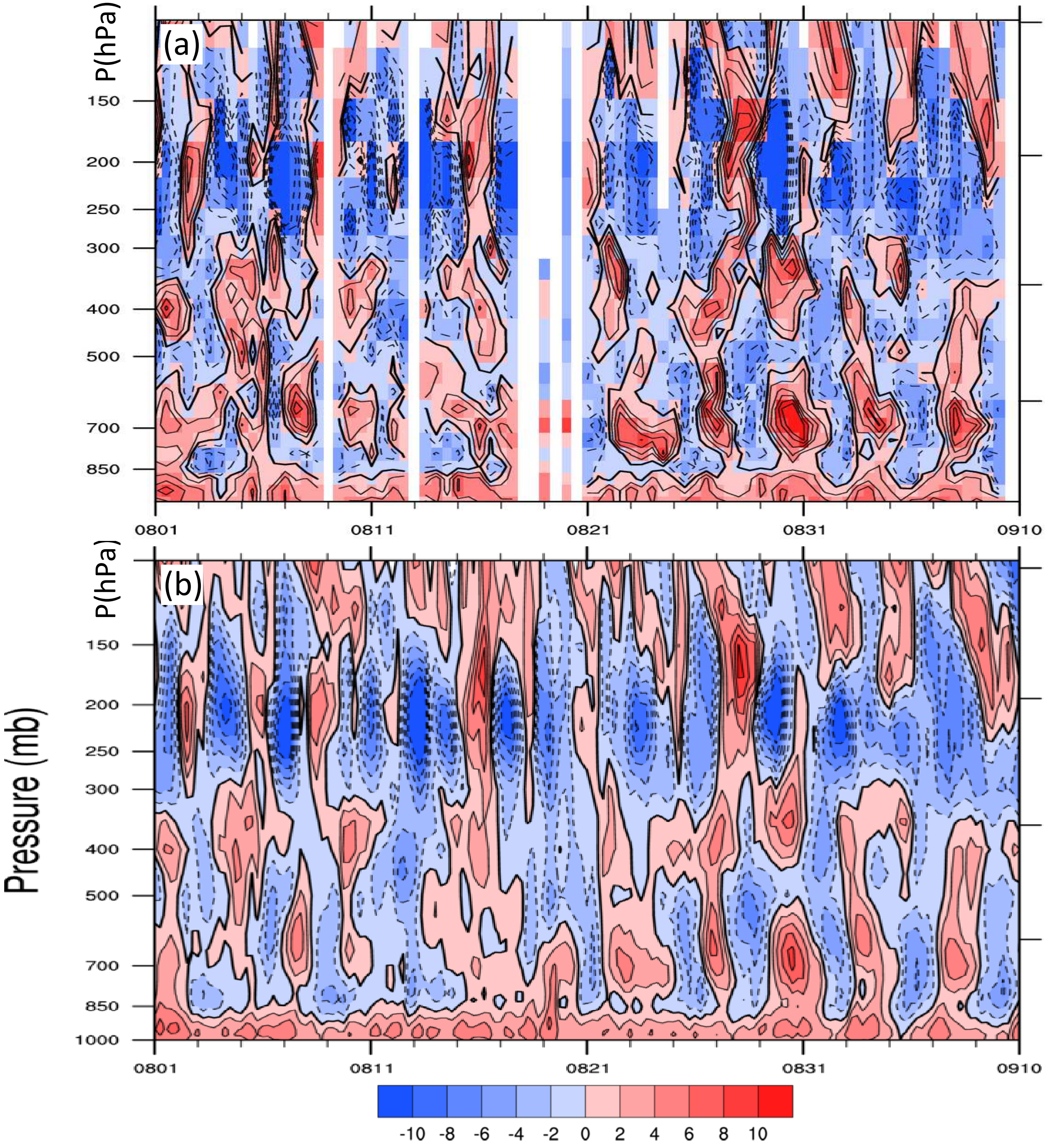

Figure 9: Evolution between the 1st August and the 10th September of the vertical profile of meridional wind (m s^{-1}) (a) observed twice a day at Abidjan [5.18°N, 4°W], and (b) averaged in the [0° – 10°N] band at the same longitude (4°W) from ERA-I reanalysis.

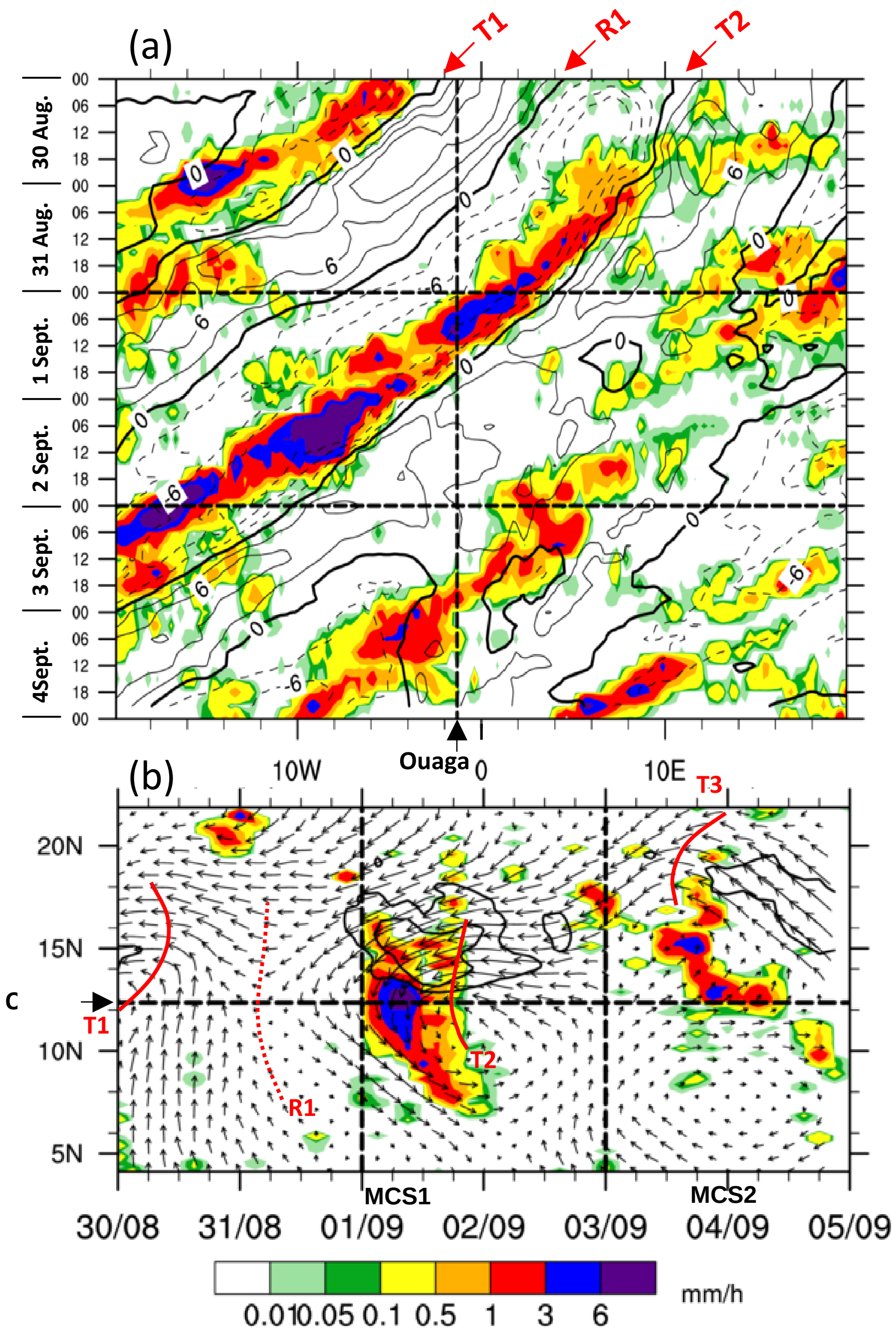

Figure 10: (a) Longitude-time and (b) latitude-time diagrams of 3-hour accumulated TRMM rainfall (colour in mm h^{-1}) from 30th August to 4th September. The meridional wind at 700 hPa (isoline in ms^{-1}) of the ARPEGE reanalysis is superposed in panel (a), with northerlies dashed. Horizontal wind vector at 700 hPa is added to panel (b) with isolines of intensity at 15 and 20 ms^{-1} to outline the AEJ core. Fields are averaged in the [10 – 14°N] latitude-band for (a) and in the [2.5°W – 0.5°W] longitude-band for (b) surrounding Ouagadougou. The longitude and latitude of Ouagadougou are indicated by vertical and horizontal dashed lines on panels (a) and (b), respectively. Troughs T1 and T2, and ridge R2 are indicated and labelled in red on both figures.

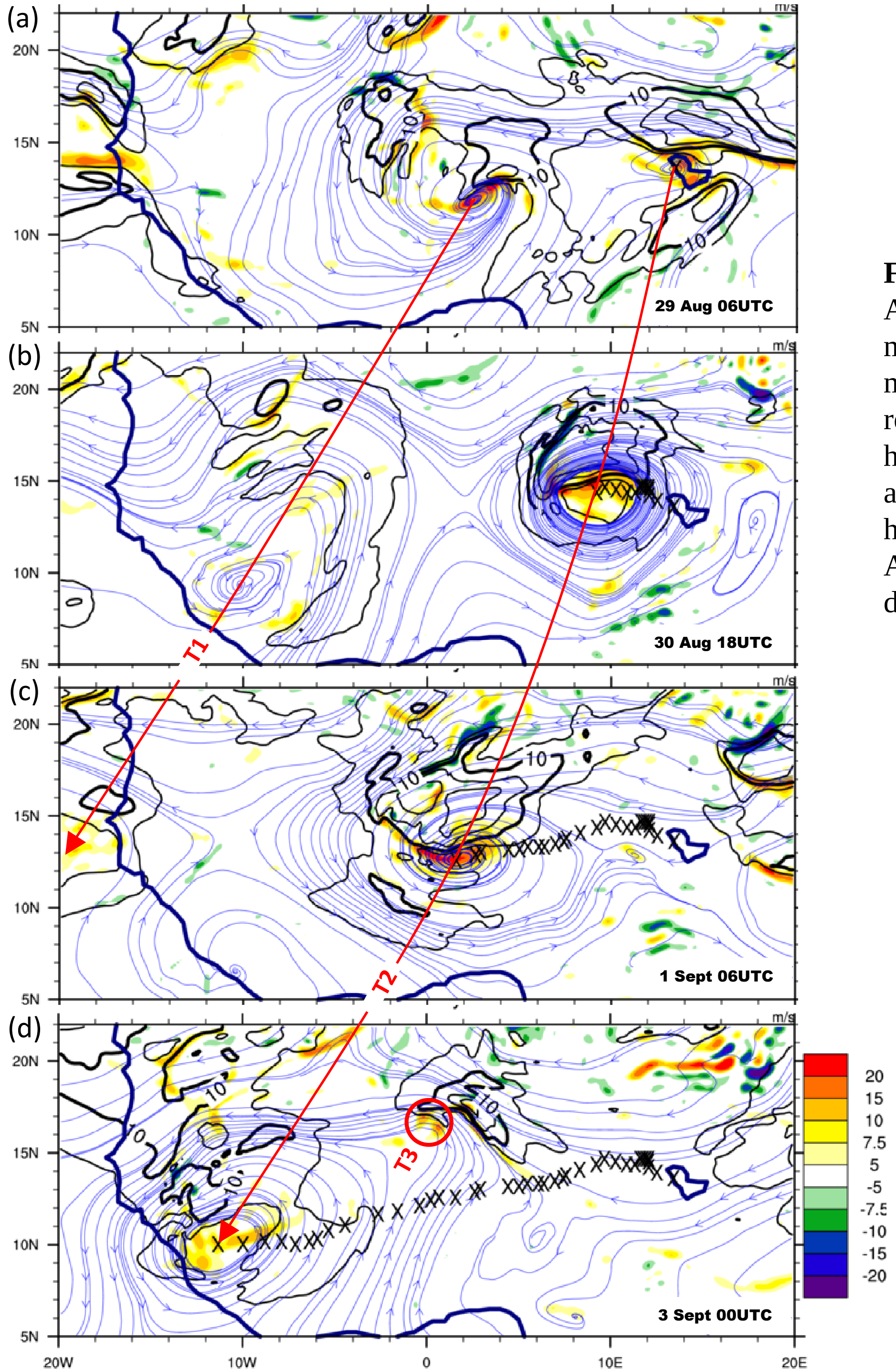

Figure 11: Tracking of the vortex associated with AEW2 for the ARPEGE reanalysis as visualized by the streamlines (blue) for the mean flow mass-weighted averaged in the 950-600 hPa layer, with mean horizontal wind speed (back isolines above 7.5 ms^{-1}) and relative vorticity (colour, 10^{-5} s^{-1}). The analysis is performed at a 36 hour interval between the 29th August at 06 UTC and 3rd September at 00 UTC. Crosses indicate the location of the vortex centre every 3 hours, whereas the red arrows show the progression of the AEW1 and AEW2 troughs. The red circle on panel (d) corresponds to the first detection of T3.

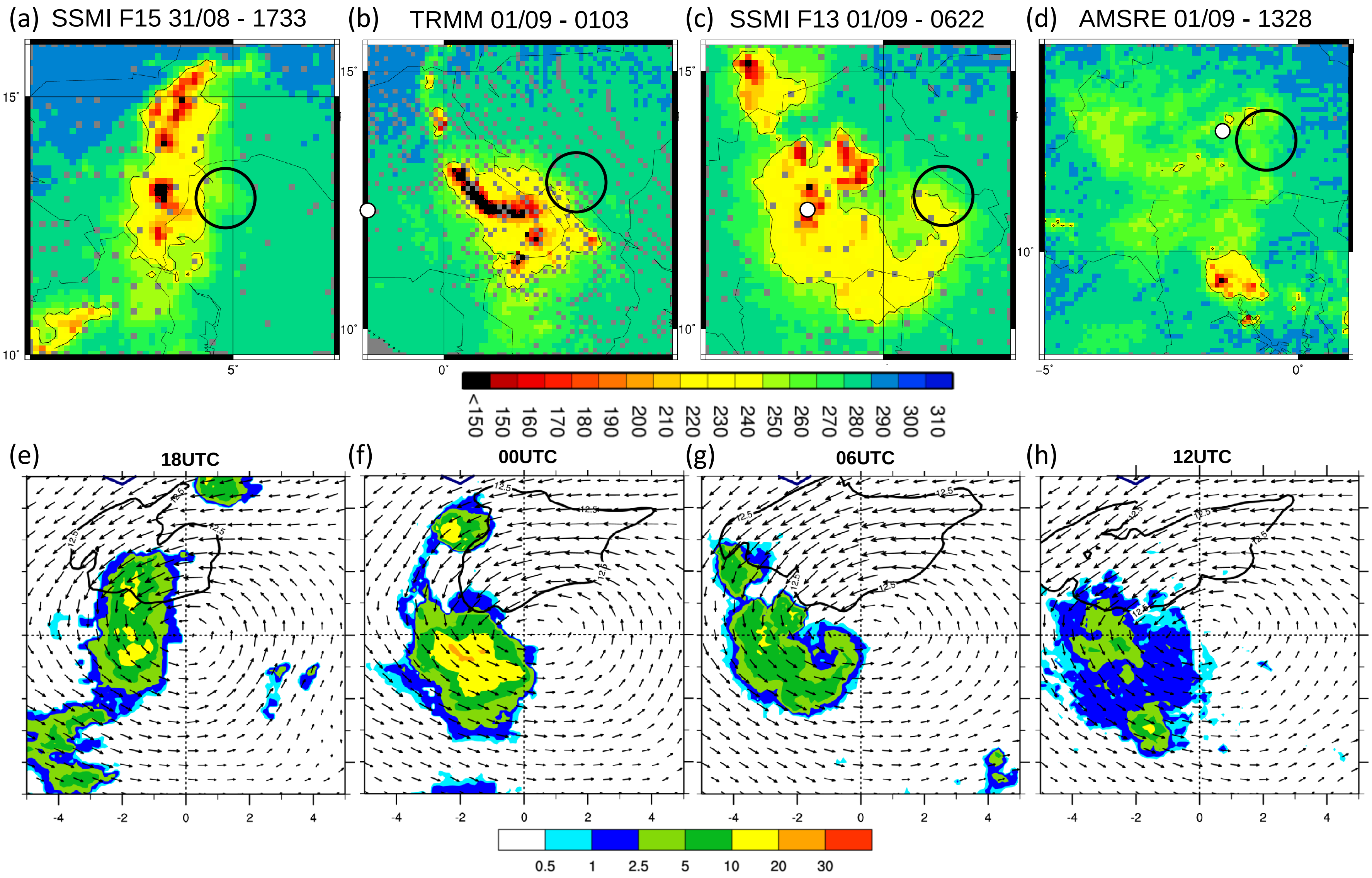

Figure 12: Upper row (a to d): satellite snapshots of the Polarized Corrected Temperature (PCT in °K) in the vortex vicinity indicated by the black circle (times are UTC). Light precipitation (1-3 mm/h) is delimited by PCT > 255 K (green shading), while convective precipitation (10-12 mm/h) correspond to PCT < 225 K (warm shading). The white dot corresponds to the Ouagadougou location. The black circle indicates the location of the mean vortex centre as detected by the ARPEGE reanalysis.
Lower row (e to h): one-day evolution at a 6 hour frequency from 31st September at 18 UTC of the GSMAP accumulated rain over 1 hr (colour in mm) and of the mean wind vector field over the 950-600 hPa layer as analysed by ARPEGE. Maps are drawn relative to the mean vortex centre in a 10° square domain. Heavy black contours outline wind speed higher than 12.5 ms^{-1}.

A multi-scale analysis of the extreme rain event of Ouagadougou in 2009

by

J-P. Lafore, F. Beucher, P. Peyrillé, A. Diongue-Niang, N. Chapelon, D. Bouniol, G. Caniaux, F. Favot, F. Ferry, F. Guichard, E. Poan, R. Roehrig and T. Vischel*

This Ouagadougou extreme event (263 mm) corresponds to the passage of an African easterly wave train combined with a strong and large wet anomaly initiated over Eastern-Africa, resulting in its breaking and the formation of a moist vortex forcing intense precipitations. Contrary to squall lines, this system is not associated with density currents and propagates slowly allowing strong precipitation accumulation. At larger scales interactions between several equatorial waves (Kelvin and Rossby) contributed to the occurrence of this event.